Pangenomic classification of pituitary neuroendocrine tumors

Mario Neou, Chiara Villa, Roberta Armignacco, A. Jouinot, Marie-Laure Raffin-Sanson, A. Septier, Franck Letourneur, Ségolène Diry, Marc Diedisheim, Brigitte Izac, et al.

Version of Record: https://www.sciencedirect.com/science/article/pii/S1535610819305227
Manuscript_3f29a65e548c035c2b0b9bac84e0be6c

Pangenomic classification of pituitary neuroendocrine tumors

Mario Neou[1-3,16], Chiara Villa[1-5,16], Roberta Armignacco[1-3], Anne Jouinot[1-3], Marie-Laure Raffin-Sanson[6-7], Amandine Septier[1-3], Franck Letourneur[1-3,8], Ségolène Diry[1-3], Marc Diedisheim[9], Brigitte Izac[1-3,8], Cassandra Gaspar[1-3,10], Karine Perlemoine[1-3], Victoria Verjus[1-3], Michèle Bernier[4], Anne Boulain[11], Jean-François Emile[12], Xavier Bertagna[1-3,13], Florence Jaffrezic[14], Denis Laloe[14], Bertrand Baussart[15], Jérôme Bertherat[1-3,13,17], Stephan Gaillard[15,17], and Guillaume Assié[1-3,13,17,18*]

1. INSERM U1016, Institut Cochin, Paris, 75014, France.
2. CNRS UMR 8104, Paris, 75014 France.
3. Université Paris Descartes-Université de Paris, Paris, 75006, France.
4. Department of Pathological Cytology and Anatomy, Foch Hospital, Suresnes F-92151 Paris, France.
5. Department of Endocrinology, Sart Tilman B35, 4000 Liège, Belgium
6. Department of Endocrinology, Hôpital Ambroise Paré, Assistance Publique–Hôpitaux de Paris, Boulogne Billancourt, Paris, 92100, France,
7. UE4340, Université de Versailles Saint-Quentin-en-Yvelines Montigny-le-Bretonneux, Versailles, 78000, France
8. Plate-Forme Séquençage et Génomique (Genom'IC), INSERM U1016, Institut Cochin, Paris, 75014, France.
9. Department of Diabetology, Assistance Publique–Hôpitaux de Paris, Hôpital Cochin, Paris, 75014, France
10. Sorbonne Université, Inserm, UMS PASS, Plateforme Post-génomique de la Pitié-Salpêtrière, P3S, F-75013, Paris, France
11. Department of Diagnostic and Interventional Neuroradiology, Foch Hospital, Suresnes, F-92151, France
12. Department of Pathology, Ambroise Paré, Assistance Publique–Hôpitaux de Paris, Boulogne Billancourt, Paris, 92100, France,
13. Department of Endocrinology, Center for Rare Adrenal Diseases, Assistance Publique–Hôpitaux de Paris, Hôpital Cochin, Paris, 75014, France.
14. INRA, UMR 1313 GABI, Université Paris Saclay, AgroParisTech, Jouy-en-Josas, 78352, France
15. Department of Neurosurgery, Foch Hospital, Suresnes, F-92151, France
16. These authors contributed equally
17. Senior author
18. Lead Contact

* Correspondence: guillaume.assie@aphp.fr

Summary

Pituitary neuroendocrine tumors (PitNETs), are common, with five main histological subtypes: lactotroph, somatotroph, and thyrotroph (*POU1F1*/PIT1 lineage); corticotroph (TBX19/TPIT lineage); and gonadotroph (NR5A1/SF1 lineage). We report a comprehensive pangenomic classification of PitNETs. PitNETs from *POU1F1*/PIT1 lineage showed an epigenetic signature of diffuse DNA hypomethylation, with transposable elements expression and chromosomal instability (except for *GNAS*-mutated somatotrophs). In TPIT lineage, corticotrophs were divided in three classes: the *USP8*-mutated with overt secretion, the *USP8*-wild-type with increased invasiveness and increased epithelial-mesenchymal-transition, and the large silent tumors with gonadotroph trans-differentiation. Unexpected expression of gonadotroph markers was also found in *GNAS*-wild-type somatotrophs (SF1 expression), challenging the current definition of SF1/gonadotroph lineage. This classification improves our understanding and impacts clinical stratification of patients with PitNETs.

Keywords

Pituitary Neuroendocrine Tumors (PitNETs), genomic, transcriptome, exome, methylome, miRnome, chromosome alterations, outcome.

Significance

PitNETs are common, with important morbidity. We report a multi-genomic characterization of PitNETs, based on a series of 134 tumors covering the whole clinical spectrum. Pituitary lineage was the main determinant of unsupervised genomic classification (before aggressiveness). New molecular entities were identified, impacting prognosis and treatments. Diffuse DNA hypomethylation was identified in *POU1F1*/PIT1 lineage. The association with chromosomal instability and expression of transposable elements points towards an original association of genomic instability with lineage differentiation (and not with aggressiveness). Furthermore, gonadotroph markers were identified in subsets of corticotrophs and somatotroph PitNETs, blurring the current limits of gonadotroph lineage.

These valuable genomic data are available to the community and should pave the way to several future clinical and pathophysiological studies.

Introduction

Pituitary neuroendocrine tumors (PitNETs), affect up to 5% of the general population (Asa et al., 2017). The most common PitNETs belong to the lactotroph lineage, followed by gonadotroph, somatotroph, corticotroph, and, more rarely, thyrotroph-lineage tumors, which express and/or secrete prolactin, gonadotrophins, growth-hormone (acromegaly), corticotrophin (Cushing's disease), and thyrostimulin (central hyperthyroidism), respectively. Endocrine diseases related to these secretions induce an important morbidity, potentially leading to death in case of severe and uncontrolled secretion. A majority of PitNETs develop locally. Some PitNETs invade or compress adjacent structures and, more rarely, give rise to metastases (Molitch, 2017). Recently, the term “adenomas” referring to these tumors was changed for “PitNETs”, better reflecting this potential loco-regional and distant aggressiveness (Asa et al., 2017).

First-line treatment includes pituitary surgery, along with medical treatment for specific PitNETs subtypes: dopamine agonists for lactotrophs and somatostatin analogs for somatotrophs. Radiotherapy and systemic chemotherapy may also be proposed (Molitch, 2017). When complete surgery is not achievable, the prognosis of a remaining tumor cannot be established from clinical or pathological data. Histo-prognostic classification of PitNETs is a subject of debate (Rindi et al., 2018). World Health Organization (WHO) released its latest histo-prognostic classification in 2017 (Lloyd et al., 2017).

Pituitary tumorigenesis is still poorly understood. Rare monogenic familial PitNETs are mostly related to *MENIN* and *AIP* germline mutations. Recurrent somatic mutations are limited to *GNAS*, encoding the PKA-cAMP pathway activator Gsα, in somatotroph (Spada et al., 1990), and *USP8*, encoding ubiquitin-specific peptidase 8, in corticotroph (Ma et al., 2015; Reincke et al., 2015) PitNETs, both occurring in one third of cases. PitNETs have been characterized by various genomic approaches. Exome sequencing has not reported any common recurrent mutations beyond *USP8* and *GNAS* (Bi et al., 2017; Song et al., 2016). Chromosomal profiling has shown common extensive chromosomal alterations, contrasting with the generally benign behavior of PitNETs (Pack et al., 2005; Salomon et al., 2018). Transcriptome analyses have identified specific somatotroph and corticotroph signatures

(Salomon et al., 2018) and aggressiveness signatures were proposed (Salomon et al., 2018). The MiRnome shows several differentially expressed miRNAs (Bottoni et al., 2007; Cheunsuchon et al., 2011). The DNA methylome shows differentially methylated genes (Duong et al., 2012; Salomon et al., 2018) and discrepant methylation patterns between functioning and non-functioning PitNETs (Ling et al., 2014; Salomon et al., 2018). Most studies have consisted of mono-omic analyses and supervised comparisons, based on disputable clinical and morphological criteria. However, one recent study by Salomon et al. integrated exome, methylome, and transcriptome analyses in a series of 37 PitNETs, including somatotroph, corticotroph and non-functional PitNETs (Salomon et al., 2018).

Beyond PitNETs, various other types of human tumors have been extensively explored using pangenomics, providing highly valuable sources of data for a better understanding of these tumors and the development of new therapies (Cancer Genome Atlas Research Network et al., 2013; Zhang et al., 2019). In contrast, PitNETs have not yet been properly characterized. Here, we combined various omics analyses on a series of 134 PitNETs of high quality and purity, carefully collected from a single expert center. We included all histological, secretory, and aggressiveness types, with extensive clinical characterization. Our aim was to provide a molecularly unbiased classification, further deciphering the pathways responsible for tumorigenesis and providing extensive molecular data from a single set of PitNETs.

Results

Patients with PitNETs

A total of 134 patients were included (Table S1), with a similar number of female and male patients, a median age of 49 y.o. (range: 15 to 84). Median tumor size was 20 mm (range: 6 to 50). This series covered all PitNETs types, including 35 (26%) corticotroph, 29 (22%) gonadotroph, 23 (17%) somatotroph, 16 (12%) lactotroph, and 8 (6%) mixed GH-PRL PitNETs. Rare types were also represented, including 8 (6%) null-cell, 6 (4%) thyrotroph and 9 (7%) plurihormonal PIT1-positive PitNETs. Different levels of aggressiveness were also represented, including 60 (45%) patients in remission after surgery, 48 (36%) patients with persistent disease, 12 (9%) patients with resistant disease and 14 (10%) patients with aggressive disease (Table S1).

Mutations and chromosomal alterations in PitNETs

The mutational landscape was established by combining exome and RNA sequencing (n = 83) or RNA sequencing alone (n = 51). Only two genes, *GNAS* and *USP8*, were found mutated in >5% of PitNETs, as previously reported (Bi et al., 2017; Song et al., 2016) (Table S2). The median number of somatic mutations per sample was 67 (14 to 247), with mainly C > T transitions (80%) and trinucleotide mutational "signature 1" (84%), as previously reported (Bi et al., 2017; Song et al., 2016). There was no difference between histological types (data not shown).

We identified chromosomal alterations in 86 PitNETs by SNP array. A mean of 23% of the genome was altered (0 to 100%; Table S3). Three profiles were identified: (i) PitNETs with extended chromosomal losses, (ii) PitNETs with a quiet genome, and (iii) PitNETs with extended chromosomal gains (Figure 1A-C). The number of alterations varied depending on secretion type (Anova p value < 10^{-4}), with less alterations in silent tumors (7% in gonadotroph and null-cell and 1% in silent corticotroph PitNETs), compared to secreting tumors (51% in thyrotroph, 49% in lactotroph, 32% in secreting corticotroph, 22% in plurihormonal PIT1-positive and 18% in somatotroph; Figure 1D). Chromosomal alterations were not related to aggressiveness, neither in the whole cohort (Chi^2 p =

0.21; Figure 1D), nor in any histological type (data not shown). Homozygous deletions and focal amplicons were limited (Table S3).

Epigenetic profiling of PitNETs

The miRnome of 111 PitNETs was generated by miRNA sequencing. Twelve miRNA clusters with at least five miRNAs were identified, combining physical proximity on the genome and correlation of their expression (Figure 2A, Table S4). Unsupervised classification based on non-negative matrix factorization identified four groups (miR1 to miR4; Figure 2B, C, Table S5), strongly associated with tumor type and secretion (Chi^2 p values < 10^{-35} and <10^{-33}, respectively). In particular, *POU1F1*/PIT1 lineage tumors were distinct from gonadotroph and corticotroph PitNETs (Figure 2B, Table S5). The largest miRNA cluster, MEG3 (85 miRNAs) (Cheunsuchon et al., 2011), was associated with secretion (ANOVA p values < 10^{-25} ; Figure 2C and 2D), with higher expression in *POU1F1*/PIT1 PitNETs. An opposite expression pattern was observed for the second largest miRNA cluster, MiR532-let7 clusters (17 miRNAs), also associated with secretion (ANOVA < 10^{-14}; Figure 2C and 2D).

The methylome of 86 PitNETs of all types was determined by DNA-chip experiments. Unsupervised classification using collapsed CpGs (Table S6) and consensus clustering identified three groups (Met1 to Met3; Figure 3A, B) associated with tumor type and secretion (Chi^2 p values < 10^{-18} and < 10^{-22}, respectively). In particular, *POU1F1*/PIT1-lineage tumors showed global hypomethylation, mainly in "open sea" DNA (Figure 3C and D). Among genes that modulate DNA methylation, expression of the demethylating enzyme TET2 showed the strongest correlation with methylation in "open sea" DNA (Pearson r = -0.4; data not shown). We next studied the link between DNA methylation and chromosomal alterations. *GNAS*-mutated PitNETs showed a combination of hypomethylation and a limited number of chromosomal alterations, whereas other PitNETs showed a negative correlation between DNA methylation and chromosomal alterations (Figure 3E; Pearson r = -0.39). In these tumors, considering transposable elements (TEs) differentially expressed between PIT1-positive and PIT1-negative PitNETs, TE expression was higher in hypomethylated tumors (Pearson r = -0.55;

Figure 3F, Table S7). In a representation of PitNETs combining DNA methylation, chromosomal alterations, and TE expression, PitNETs of the *POU1F1*/PIT1 lineage were clustered in a group with hypomethylation, genome alterations, and TE overexpression (Figure 3G). We may speculate that DNA hypomethylation in the *POU1F1*/PIT1 lineage may induce chromosomal alteration through the activation of TEs, as reported in cancer (Anwar et al., 2017), but this remains to be investigated.

DNA methylation negatively correlated with the cis-expression of 1,164 genes (Pearson $r < -0.5$; Table S8). These genes were enriched in sex steroid-response and protein-secretion signatures (GSEA normalized enrichment scores > 2.8). Unsupervised transcriptome classification using these 1,164 genes generated a PitNET classification strongly reflecting methylome classification and the *POU1F1*/PIT1 lineage (Chi^2 p value $< 10^{-15}$, data not shown). Five miRNA features negatively correlated with DNA methylation in cis (Pearson $r < -0.5$), including the MEG3 cluster, reflecting its maternal imprinting, and four miRNAs reflecting the *POU1F1*/PIT1 lineage (miR-574, miR-195, miR-497-5p and let-7b).

PitNETs transcriptome

We determined the transcriptome of 134 PitNETs by RNA sequencing. Unsupervised classification based on non-negative matrix factorization revealed six distinct groups (t1 to t6; Figure 4A and 4B). These groups were associated with the 2017 WHO histo-prognostic classification (Chi^2 p value $< 10^{-68}$), with four noticeable discrepancies. First, the WHO «null-cell subtype» was not distinct from gonadotroph tumors in t4 (Figure 4A). Second, two types of corticotroph PitNETs were identified, with overt Cushing microadenomas in t1 and silent corticotroph macroadenomas in t3 (t-test p value = 0.02 for size; Chi^2 p value $< 10^{-4}$ for secretion). Third, mixed GH-PRL clustered together with somatotroph PitNETs in t6, apart from lactotroph tumors, found clustered in t2. Finally, sparsely granulated somatotroph PitNETs were mainly found in t5, with thyrotroph and plurihormonal PIT1-positive PitNETs, instead of being clustered with other somatotroph PitNETs in t6 (5/8, Chi^2 p value = 0.016; Figure 4A).

Genes driving the transcriptome showed noticeable expression signatures in each transcriptome group (Table S9). Enrichment analysis showed high cell cycle and low inflammation in t1 (overt Cushing corticotrophs), high MYC targets in t2 (lactotrophs), low epithelial-mesenchymal transition in t3 (silent corticotrophs), high oxidative phosphorylation in t4 (gonadotrophs), and high interferon alpha and gamma in t5 and t6 (thyrotrophs and somatotrophs)(Gene Set Enrichment Analysis (GSEA) hallmark FDR p values < 0.05, with normalized enrichment scores > 3; enrichment data not shown). *USP8*-and *GNAS*-mutated PitNETs were associated with specific transcriptome subgroups in the t1 and t6 transcriptome groups, respectively (Chi^2 p values < 10^{-4} and 0.02, respectively; Figure 4A), with specific signatures distinct from those of their wild-type counterparts (Table S9). Mutation of *USP8* was associated with signatures of low expression of oxidative phosphorylation, MYC targets, inflammation, and epithelial-mesenchymal transition (Table S9).

The cell composition and differentiation of each PitNET was estimated using a canonical transcriptome signature for each pituitary endocrine cell type (Table S10). Forty-five PitNETs (34%) showed a mixture of ≥ 2 cell types (Figure 4C, Table S11), mostly GH-PRL PitNETs, featuring a separated somatotroph and lactotroph compartment. Remarkably, silent corticotroph PitNETs (7/8, 88%) displayed both corticotroph and gonadotroph signatures (t3 cluster; Figure 4C), as previously suggested by some authors (Cooper et al., 2010; Suzuki et al., 2008). This was confirmed by the shared expression of gonadotroph marker GATA3 (Mete et al., 2019) by immunohistochemistry (Figure 4D). The diffuse positivity for GATA3, ACTH, and TPIT in these tumors suggests their co-expression by the same tumor cells (Figure 4D). Finally, most sparsely granulated somatotroph and plurihormonal PIT1-positive PitNETs (5/8 and 5/9, respectively) displayed a thyrotroph signature (t5 cluster; Figure 4C).

Among transcription factors (Figure 4E, Table S9), gonadotroph marker *NR5A1* (SF1) was also expressed in a subset of somatotroph PitNETs, corresponding to those with no *GNAS* mutation (Chi^2 p value = 0.003; Figure 4E).

Pangenomic classification of PitNETs

Somatic mutations, chromosomal alterations, and the miRNome, methylome, and transcriptome (Tables S1-S6 and S9) were combined into a single analysis, using multiple-factor analysis. This multi-omic projection of PitNETs identified the *POU1F1*/PIT1 lineage as the main separator (Figure 5A and 5B). Transcriptome classification combined with *GNAS*/*USP8* mutations statuses better fit the molecular groups than the 2017 WHO histo-prognostic classification (Figure5A and 5B; Bayesian Information Criterion (BIC) values: -7.723 and -6.265 for the 2017 WHO and the transcriptome classifications respectively).

Clinical relevance of pangenomic classification

In corticotroph PitNETs from t1 transcriptome group, *USP8*-wild-type PitNETs appeared more aggressive, compared to *USP8*-mutated PitNEts (Fisher exact p value = 0.018; Figure 4A). In these tumors, sphenoid invasion was more common (Fisher exact p value = 0.007). In contrast, there was no difference for cavernous invasion (Fisher exact p value =1), nor for MIB1/Ki67 labeling index (Wilcoxon p value = 0.26). The increased invasiveness of *USP8*-wild-type PitNETS was further supported by their transcriptome signature, showing an increased epithelial-mesenchymal-transition signature (GSEA hallmark FDR p value $<10^{-3}$; Figure 6A, Table S9).

Somatostatin agonists are major treatments for somatotroph PitNETs, and also used for corticotroph PitNETs (Molitch, 2017). Somatostatin receptor subtypes showed variable expression between molecular groups (Kruskal Wallis p value $<10^{-13}$ and $<10^{-15}$ for *SSTR2* and *SSTR5* respectively; Figure S1A and Figure 6B, Table S9). Notably, for corticotroph PitNETs, expression of *SSTR5* was higher in *USP8*-mutated PitNETs compared to *USP8*-wild-type (Wilcoxon p value $<10^{-4}$; Figure 6B), supporting a potential value of *USP8* mutation status for predicting response to Pasireotide as previously suggested (Hayashi et al., 2016). Dopamine receptor 2 (*DRD2*) showed the highest expression in lactotroph PitNETs (t2), followed by gonadotroph PitNEts (t3) as recently suggested (Ben-Shlomo et al., 2017) (Figure S1B). Of note Dopamine receptor 2 expression was quite variable among somatotroph PitNETs, with higher expression in *GNAS*-mutated PitNETs (Fisher exact p value

= 0.001), supporting a potential value of *GNAS* mutation status for predicting response to dopamine agonists in somatotroph PitNETs.

Temozolomide is currently recommended for treating aggressive PitNETs not responding to other treatments (Raverot et al., 2018). Temozolomide is degraded by MGMT (O-6-Methylguanine-DNA Methyltransferase) (Hegi et al., 2005). *MGMT* expression varied among molecular groups (Kruskal-Wallis p value $<10^{-4}$), but also within groups, and was not associated with aggressiveness (Kruskal-Wallis p value = 0.52; Figure 6C, Table S9). The association between *MGMT* expression and response to Temozolomide could be evaluated in three patients. Expression level was high in one not responding, intermediate in one with partial response, and low in one with complete response (Figure 6C). No negative correlation was found between *MGMT* expression and DNA methylation in *MGMT* locus, including its promoter (median correlation coefficient 0.55; range: -0.27 to 0.76). Thus *MGMT* mRNA expression level could be a predictor of Temozolomide response, in line with a previous publication using MGMT immunohistochemistry (Bengtsson et al., 2015), but not reproduced so far.

Discussion

This study provides a pangenomic classification of PitNETs. All histological types were represented, including subtypes scarcely or even unavailable in previously reported molecular studies, especially lactotroph, thyrotroph and plurihormonal PIT1-positive PitNETs. All secretion intensities and all levels of aggressiveness were represented as well, thus providing a comprehensive picture of PitNETs. This cohort was very carefully characterized clinically, both at hormonal and pathological levels, using the most advanced expertise. Collecting such samples at a high quality -pure undegraded frozen material- was challenging, owing to small size and rarity of some subtypes.

Current classifications are empirical, based mainly on histological criteria (Lloyd et al., 2017; Raverot et al., 2018). This unbiased molecular classification largely confirms the 2017 WHO classification, underlining the biological relevance of pituitary lineage factors for classifying PitNETs as decided for the 2017 WHO classification. However, in terms of clinical relevance, identifying aggressive potential and predicting the response to medical treatments are still unmet challenges. This extensive molecular study helps progress towards this goal. Indeed, the limited propensity for sphenoid invasion and limited epithelial-mesenchymal-transition of *UPS8*-mutated corticotroph PitNETs supports using the somatic genotyping of *USP8* for determining the outcome. *USP8* mutation status could also help predicting response to Pasireotide, since the molecular group of *USP8*-mutated corticotroph PitNETs showed higher SST5 expression. Finally, low mRNA level of *MGMT* could be used for predicting response to Temozolomide. Further clinical studies should now confirm these findings.

This study questions the current definition of gonadotroph lineage. Indeed, the molecular group of gonadotroph PitNETs (t4) also included null-cell PitNETs, showing that the definition of gonadotroph PitNETs should be extended to this type of PitNETs not expressing SF1. In addition, the molecular group of silent corticotroph PitNETs (t3) showed a gonadotroph signature. Previous studies also reported the expression of gonadotroph markers in a subset of corticotroph PitNETs (Cooper et al., 2010; Suzuki et al., 2008). Whether these PitNETs arise from a specific pituitary lineage distinct from other corticotroph PitNETs remains to be determined. In mouse models, distinct pituitary cell lineages expressing TPIT and proopiomelanocortin have been reported (Drouin, 2016). Finally, expression of SF1 was found in *GNAS*-wild-type somatotroph (t6b), raising the question of specificity of SF1 as a

marker of gonadotroph lineage. Taken together, these results point to limits in the current knowledge on cytodifferentiation of pituitary tumor cells.

PIT1 appeared as the main classification driver. The *POU1F1*/PIT1 lineage was associated with DNA hypomethylation, the transcription of differentiation markers, of transposable elements and chromosomal instability. It is possible that *POU1F1*/PIT1 differentiation may be associated with an epigenetic switch that induces hypomethylation, potentially via TET2, reflecting the recently reported epigenetic switch of TET1 in the gonadotroph lineage (Yosefzon et al., 2017). Functional studies will help to understand the direct impact of *POU1F1*/PIT1 on DNA methylation and more generally on chromatin structure, and subsequently the underlying mechanisms.

Beyond *USP8* and *GNAS* mutations, no obvious driver alteration was identified for a majority of PitNETs. Especially a group of 24 PitNETs showed no functional somatic variant and no chromosome alteration. Most of these PitNETs were silent (21/24, 87%), including mainly gonadotroph and all null-cell (16/24, 66%), and silent corticotroph (4/24; 17%) PitNETs. For these PitNEts, a technical failure of genomic alteration detection is unlikely, given the high purity of these samples -inferred from transcriptome signatures (Figure 4C). Further characterization of these PitNETs with techniques such as whole genome sequencing coupled to chromatin structure analyzes may unravel mutations in non-coding regions impacting chromatin opening and/or the binding of specific transcription factors.

In conclusion, this study showed a robust unbiased molecular classification, with new subtypes not previously characterized. The biological mechanisms identified here and the potential clinical applications should lead to important improvements in understanding the biology of these tumors, and in managing patients with these tumors.

Acknowledgements

This work was funded by La Fondation Foch and supported by the Assistance Publique Hôpitaux de Paris (VF grant). We thank the genomic platform of Cochin Institute (Paris) and the Post-Genomic Platform of Sorbonne University (Paris), where the genomic data were generated.

Author contributions

J.B., S.G., C.V., X.B., and G.A.: conceptualization. C.V. and M.B.: investigation (pathology review). C.V., M.L.R.S., V.V., A.B., B.B., S.G. and G.A.: resources (clinical data). M.L.R.S., J.F.E., C.V., J.B., S.G. and G.A.: project administration (ethical aspects management). B.B. and S.G.: resources (Human pituitary samples collection). K.P. and C.V.: investigation (samples handling). F.L., B.I. and C.G.: investigation (genomic data generation). M.N., R.A., A.J., A.S, S.D., F.J., D.L., M.D. and G.A.: formal analysis (bioinformatic and statistical analyses). M.N., C.V., A.S., A.J., R.A., X.B. and G.A.: writing – original draft preparation. All authors: writing – review and editing.

Declaration of interests

The authors declare no competing interests.

Figure legends

Figure 1. Chromosomal alterations in PitNETs. (A) Cumulative proportions of chromosomal gains and losses for each indicated patient tumor. (B) Cumulative proportions of chromosomal gains and losses by chromosomal location. (C) Heatmap of chromosomal losses and gains in PitNETs. (D) Pathological and clinical annotations. The association with chromosomal alteration groups is provided (p (χ2): chi-square p values).

See also Tables S1-S3.

Figure 2. The miRNome of PitNETs. (A) miRNA clusters in PitNETs: miRNA clusters were defined as consecutive miRNAs showing correlated expression among samples. Correlations are coded in the red scale. Clusters are presented in blue. (B) Unsupervised clustering of PitNETs based on their miRnome profile, using four NMF (non-negative matrix factorization ranks). The heatmap encodes the values of the H decomposition matrix.. (C) Pathological and clinical annotations. The association with miRNA groups is provided (p (χ2): chi-square p values). (D) Expression heatmap of the most differentially expressed miRNA between the miRNome groups. DESeq normalized counts are provided.

See also Tables S4 and S5.

Figure 3. Methylome of PitNETs. (A) Unsupervised hierarchical clustering of PitNETs based on their methylome profile. Pathological and clinical annotations are provided. The association with methylome groups is detailed (p (χ2): chi-square p values). (B) Methylation heatmap of the top 2,500 most variable CpG features. Beta-values are reported. *Normal tissue beta-value refers to the mean

beta-value of “backbone” CpGs (intergenic and open sea CpGs), previously assessed to be approximately 0.8 in 21 normal tissues (Lee and Wiemels, 2016).

(C) Repartition of hypomethylated (in blue) and hypermethylated (in red) CpGs in *POU1F1*/PIT1-positive PitNETs *versus* *POU1F1*/PIT1-negative PitNETs. (D) Scatterplot of *POU1F1* expression (x-axis) and DNA methylation (y-axis; median beta-values of open sea-related CpG clusters). (E) Scatterplot of DNA methylation (x-axis) and chromosomal alteration (y-axis). (F) Scatterplot of DNA methylation (x-axis) and transposable element (TE) expression (y-axis). **Normalized TE expressions are provided for each sample, generated by aggregating the expression of all differentially expressed TEs (between *POU1F1*/PIT1-positive and *POU1F1*/PIT1-negative PitNETs) into a single TE expression value, subsequently normalized by DESeq, after including all other transcripts. (G) Principal-component analysis of DNA methylation, genome alteration and TEs. PitNETs are projected following components 1 and 2.

See also Tables S6-S8.

Figure 4. Transcriptome of PitNETs. (A) Unsupervised classification of PitNETs identifies six main groups, corresponding to corticotroph with overt Cushing (t1), lactotroph (t2), silent corticotroph (t3), gonadotroph (t4), thyrotroph (t5), and somatotroph (t6) PitNETs. Pathological and clinical annotations are provided. The association with transcriptome groups is detailed (p (χ2): chi-square p values). (B) Heatmap of the six NMF ranks used for generating the unsupervised classification. (C) Proportion of gonado-, cortico-, somato-, lacto- and thyrotroph canonical signatures in each PitNET. (D) 20x magnification of hematoxylin/eosin staining and immunohistochemistry for the corticotroph-related markers ACTH and TPIT and the gonadotroph-related markers SF1 and GATA3 performed on tissue sections of corticotroph of overt Cushing (P114), silent corticotroph (P054), and gonadotroph (P098) PitNETs. The black bar represents 100 µm. (E) Expression profiles related to the top 50 most significantly differentially expressed transcription factors among the six transcriptome groups.

See also Tables S9-S11.

Figure 5. Pangenomic classification of PitNETs. Dots represent individual PitNETs, projected according to their MFA (multiple-factor analysis) scores, which integrate all the presented –omics data. The two first axes of the MFA are presented on this figure. PitNETs are clustered following either their histological types, as defined by WHO 2017 classification (panel A), or their transcriptome groups and *USP8* and *GNAS* mutation status (panel B). For each group, the 95% inertia ellipse is represented.

Figure 6. Gene expression profiles with potential clinical impact. (A) Vulcano-plot representation of differentially expressed genes between *USP8*-mutated and *USP8*-wildtype corticotroph PitNETs from t1 transcriptome group. In red and in blue: genes over-expressed and under-expressed in *USP8*-mutated PitNETs respectively. Circled dots: genes involved in EMT (GSEA hallmark). (B) Somatostatin receptor 5 expression in PitNETs. (C) MGMT (O-6-Methylguanine-DNA Methyltransferase) expression in PitNETs. ** Mann-Whitney $p<0.0001$; * Mann-Whitney $p<0.01$; Ns, not significant; ΔΔ complete response to Temozolomide; Δ partial response to Temozolomide; # no response to Temozolomide.

See also Figure S1.

STAR methods

Lead contact and materials availability

Further information and requests for resources and reagents should be directed to and will be fulfilled by the Lead Contact, Guillaume Assié (guillaume.assie@aphp.fr).

Experimental model and subject details

Patient samples

134 patients with a PitNET were included, representing all subtypes (Table S1). All were operated by transsphenoidal surgery at the Foch Hospital, between 2007 and 2016. During surgery, tumor fragments were removed by the surgeon and small tumor specimens were carefully selected in the middle of the tumor to avoid any contamination by normal tissue, then rapidly –within 15 min- snap-frozen into liquid nitrogen and subsequently stored at -80°C. The remaining samples were formalin-fixed, and paraffin embedded for histological examination and immunohistochemical study.

Signed informed consent for molecular analysis of tumors and for access to clinical data was obtained from all patients, and the study was approved by the Ethics Committee Ile de France 8 (ID RCB 2010-A00618-31).

Extensive hormone exploration was performed before surgery following standard pituitary guidelines (Freda et al., 2011).

A pituitary MRI was performed before surgery for all patients, read by a senior radiologist (A.B.). The following criteria were assessed: size in the three dimensions (height, width and depth), cavernous sinus invasion, sphenoidal invasion, and optical chiasm status.

Method details

Tumor sample collection and characterization

Tumor samples were collected directly by the neurosurgeon (S.G. and B.B.) under endoscopy, selecting the most representative fragments with minimal contamination and necrosis. These samples were directly snap-frozen in liquid nitrogen and stored at -80°C. In parallel, for all patients, histological examination of tumor specimens was performed by senior pathologists (C.V. and M.B.), and revised by a single senior pathologist (C.V.). Histological subtype was defined according to WHO 2017 classification of endocrine tumors. The following criteria were assessed: mitotic count (mitoses/10HPF), histological invasion of dura-mater, bone tissue and respiratory mucosa, and by immunohistochemistry: ACTH, PRL, GH, FSH, LH, TSH-, along with PIT1, TPIT, GATA3, SF1, cytokeratin 8 (CAM5.2), Ki67 (MIB1), and p53, using fully automated IHC/ISH slide staining instrument BenchMark XT (Roche -Ventana Medical System, Inc.-, Tucson, AZ, USA). The antibodies features are the following:

Antibody	*Provider*	*Reference*	*Clone*	*Host Specie*	*Dilution*	*Ag-retrieval*	*Incub (min)*
ACTH	DAKO	M 3501	02A3	mouse	1/2000	None	32
Beta-LH	DAKO	M3502	C93	mouse	1/50	CC1 short	32
Beta-TSH	DAKO	M3503	42	mouse	1/300	None	20
Beta-FSH	DAKO	M3504	C10	mouse	1/50	CC1 short	32
Prolactine	DAKO	A0569	PROL	rabbit poly	1/300	None	20
hGH	DAKO	A 0570	GH	rabbit	1/3000	None	40
CAM 5.2	BECTON	345779	CAM5.2	mouse	pre-dilut	CC1 short	32
PIT-1	NOVUS BIO	NBP1-92273	POU1-F1	rabbit	1/500	CC1 standard	60
T-Pit	ATLAS AB	AMAb91409	CL6251	mouse	1/200	CC1 standard	32
SF-1	ABCAM	Ab217317	EPR19744	rabbit	1/500	CC1 long	60
GATA3	ROCHE	7604897	GATA3	mouse	pre-diluted	CC1 standard	32
Ki67	DAKO	M7240	MIB-1	mouse	1/50	CC1 short	32
p53	DAKO	M7001	DO-7	mouse	1/50	CC1 short	24

These tumor specimens were used for integrated genomic analyses, including mRNA sequencing (n=134), miRNA sequencing (n=111), exome sequencing (n=83), SNP arrays (n=86), DNA methylation arrays (n=86).

DNA and RNA extraction

Tumor samples (10–50 mg) were powdered under liquid nitrogen. DNA was extracted and purified following proteinase K digestion, using DNeasy columns (Qiagen, Hilden, Germany). DNA concentrations were determined using a Qubit 3 fluorometer (Thermofisher, Waltham, MA, USA).

RNA and miRNA were extracted using RNAble (Eurobio, Les Ulis, France) and cleaned by RNeasy column (Qiagen). Aliquots of RNA were analyzed by electrophoresis on a Bioanalyzer 2100 (version A.02 S1292; Agilent Technologies, Santa Clara, CA, USA) and quantified using a Nanodrop ND-1000 (Thermofisher). Stringent criteria for RNA quality were applied to rule out degradation.

Exome sequencing and variants calling

Whole-exome sequencing was performed using NimbleGen MedExome capture (Roche NimbleGen, Madison, WI, USA) from 1 µg of high quality genomic DNA, followed by sequencing of libraries using paired-end mode (2x 75bp) on a Nextseq 500 platform (Illumina, San Diego, CA, USA), at the Genomics Platform of the Cochin Institute. Reads were aligned on hg19 (GRCh37) using BWA V0.7.17 (Li and Durbin, 2009). Variant calling was performed using GATK V4.0.8.1 (McKenna et al., 2010). Another variant calling was generated from RNA sequencing data (Table S2). Sequence variants were annotated using ANNOVAR (April, 16th 2018) (Wang et al., 2010).

For somatic mutation counts and mutational signatures analyses, samples were included only if both exome and RNA sequencing data were available (Table S2). Variants were filtered if rare (EXac<=1%), sufficiently represented (allelic ratio ≥30%, and supported by ≥4 reads), present in RNA sequencing, and previously reported in Cosmic (Sondka et al., 2018). Mutational signatures were explored using the Wellcome Trust Sanger Institute mutational signatures framework (Alexandrov et al., 2013) implemented in the DeconstructSigs v.1.8.0 R package (Rosenthal et al., 2016). Significance of variants was further explored using MutsigCV 1.41 (Lawrence et al., 2013).

For identifying genes recurrently mutated, the whole cohort was used. Of note, for 51 samples, no exome was available. For these samples, variant calling was performed from RNA sequencing data,

using the previous criteria. Variants were further filtered if "functional" (exonic or splicing, non-synonymous and not predicted as benign by Sift and Polyphen2 annotations from ANNOVAR), and affecting genes previously reported as mutated in PitNets exomes (Bi et al., 2017; Ronchi et al., 2016; Song et al., 2016; Välimäki et al., 2015). Filtered variants were visually validated using Integrative Genome Viewer (V2.4.10) (Robinson et al., 2011). Counts of recurrence for each gene were calculated from these filtered variants (Table S2).

SNP array analysis

SNP array data were generated using the Infinium® HumanCore-24 v1.0 BeadChip (Illumina). SNP array hybridization was performed by Post-Genomic Platform of Sorbonne University following manufacturer recommendations. Genome Alteration Print (GAP) method was used to call altered chromosomal segments and to estimate the proportion of cells for each alteration (Popova et al., 2009). Consecutive segments belonging to the same alteration were merged. All chromosomal alterations were visually validated, by plotting B-allele frequency (BAF) and signal intensity LogR ratio (LRR) (data not shown).

Samples were classified into three categories "Lost", "Quiet" and "Gained", depending both on the number of alterations and the predominance of either chromosomal losses or gains (>1% of the genome lost, >1% of the genome gained and <1% of the genome altered for "Lost", "Gained" and "Quiet" respectively).

Homozygous deletions were called based on low copy number, defined by LRR lower than 3x the sample standard deviation. Amplicons were defined by ≥5 DNA copies. When genes were found in these regions, the impact on expression was assessed using a robust Z-score on RNA-sequencing data, comparing each sample with other PitNETs of similar histotype and with the entire PitNET cohort.

DNA methylation profiling

Whole-genome DNA methylation was performed at the Post-Genomic Platform of Sorbonne University, using the Infinium® MethylationEPIC BeadChip (Illumina), featuring 850,000 CpG sites.

Raw data were processed with Minfi (v1.24.0) (Aryee et al., 2014). Probes were filtered using default parameters and beta-values were extracted, then normalized with the "Funnorm" function (Fortin et al., 2014). Adjacent CpGs were collapsed into CpG features, using the "cpgCollapse" function with default parameters.

Unsupervised classification was performed with Pheatmap 1.0.10 and ConsensusClusterPlus 1.42.0 (Wilkerson and Hayes, 2010) on beta-values, using hclust function and Euclidean distance, based on top 2500 more variable CpG features (based on standard deviation after exclusion of sex chromosomes) and 5000 iterations.

MiRNA profiling

Small RNA (<100 bases in length) were purified from total RNA using miRNeasy kit (Qiagen), then sequenced. Libraries were prepared at the Genomics Platform of the Cochin Institute, following the TruSeq small RNA protocol (Illumina), starting from 1 µg of high quality total RNA. Single read (1 × 75 bp) sequencing was performed on a Nextseq 500 platform (Illumina). FASTQ sequences were aligned on miRBase v.2052, then counted with STAR (v.2.5.2a) (Dobin et al., 2013). Counts were normalized with DESeq v1.30.0 (Anders and Huber, 2010).

Adjacent miRNAs were collapsed into miRNA clusters when falling within 1 Mb and showing a Pearson correlation coefficient ≥ 0.5. A graphic representation of all miRNA clusters was generated using the LDheatmap package 0.99-5 (Shin et al., 2006). Subsequent analyses were performed using miRNA clusters, along with individual miRNAs not belonging to any cluster. Expression of miRNA clusters was represented by a tag-miRNA, selected as the one showing the highest correlation with the other miRNAs within the cluster.

The top 150 most variable miRNA clusters/individual miRNAs were selected based on their standard deviation. Groups with similar miRNA abundance profiles were identified using unsupervised non-negative matrix factorization consensus clustering using the NMF R package v0.21 (Gaujoux and Seoighe, 2010), using default parameters. The best rank was chosen from both cophenetic and average silhouette width score profiles. A clustering run was then performed, with the chosen k=4 ranks and 1000 iterations. Plots were generated with Pheatmap v1.0.10. Differential miRNA clusters/individual miRNAs between NMF groups were identified using the Kruskal-Wallis test. MiRNA transcripts targets were obtained using miRTarBase v6 (Chou et al., 2016), filtering those with experimental validation.

mRNA profiling

Total RNA was extracted using RNAble (Eurobio), cleaned-up with RNeasy columns (Qiagen) and sequenced. The libraries were prepared at the Genomics Platform of the Cochin Institute, following the TruSeq Stranded mRNA protocol (Illumina), starting from 1 µg of high quality total RNA. Paired end (2 × 75 bp) sequencing was performed on a Nextseq 500 platform (Illumina).

FASTQ sequences were aligned on hg19 (GRCh37) human reference genome with STAR (v.2.5.2a) (Dobin et al., 2013). Read-counts were aggregated by genes, then normalized with DESeq v1.30.0 (Anders and Huber, 2010).

The top 1500 most variable genes were selected, based on their standard deviation. Groups with similar mRNA abundance profiles were identified using unsupervised non-negative matrix factorization consensus clustering using the NMF R package v0.21 (Gaujoux and Seoighe, 2010), using default parameters. The best rank was chosen from both cophenetic and average silhouette width score profiles. A clustering run was then performed, with the chosen k=6 ranks and 200 iterations. Plots were generated with Pheatmap v1.0.10. Differentially expressed genes between NMF groups were identified using the Kruskal-Wallis test. For each NMF group, a gene expression signature was generated by comparing this group with all other groups, limiting the NMF group sizes to the size of

the smallest group by random sampling, using DESeq v1.30.0 (Anders and Huber, 2010). Gene-set enrichment analyses were performed using GSEA v2.2.3 (Subramanian et al., 2005) preranked method, using the hallmark annotation. The lists of transcription factors and GPCRs were obtained from *Lambert et al.* (Lambert et al., 2018) and *Alexander et al.* (Alexander et al., 2017), respectively. Transposable elements (TE) were identified after a new alignment of RNA sequencing data with STAR (Dobin et al., 2013), keeping multi-mapped reads. TE were then counted using TEToolkit V2.0.3 (Jin et al., 2015), then normalized using DESeq (including all transcripts) (Anders and Huber, 2010). TE read counts and differential expression between PIT1-positive and PIT1-negative PitNETs are provided in Table S7. TE differentially expressed were aggregated either by families, by classes or into a single TE value, by summing the corresponding read-counts. For each aggregation, a specific DESeq normalization was performed, including all mRNA transcripts in addition to aggregated TE.

Multi-omic classification

Few methods can simultaneously integrate several related datasets. Amongst them, the Multiple Factor Analysis (Escofier and Pagès, 1994; Rajasundaram and Selbig, 2016) (MFA) is widely used today. It consists of balancing the influence of different datasets in a weighted Principal Components Analysis (PCA). This method allows a general picture of the consensus among datasets to be established, as well as the relationships between consensus and single datasets to be identified. MFA was performed on 75 samples with all omics data in R software version 3.5.2 with the ade4 package (Dray and Dufour, 2007). After MFA projection, samples were labeled using either the transcriptome classification with *USP8*/*GNAS* mutation status or the WHO 2017 histo-prognostic classification. The accuracy of these two classifications were compared using Bayesian Information Criterion (BIC) values, generated with the HDclassif R package (Bergé et al., 2012).

Quantification and statistical analysis

Calculations were performed using R statistical software. Comparison between groups were assessed using parametric or non-parametric tests depending on the number of observations and the distribution for each variable. When normality assumption was verified, group comparisons were analyzed using Student's t-test or parametric analysis of variance (Anova) for quantitative variables and chi-square test for qualitative variables. In case of non-normal distribution or small number of observations, group comparisons were assessed using Mann-Whitney or Kruskal-Wallis test for quantitative variables, and Fisher's test for qualitative variables. Correlations were assessed using the Pearson coefficient.

All p values were two-sided, and the level of significance was set at $p < 0.05$.

Data and code availability

Data and Code Availability Statement

MiRNA and mRNA read counts are available at the European Bioinformatics Institute (EMBL-EBI) under accession numbers E-MTAB-7969 and E-MTAB-7768 respectively. Methylome data are available under EMBL-EBI accession number E-MTAB-7762. Sequencing data (exome, mRNA and MiRNA sequencing) has been deposited at the European Genome-phenome Archive (EGA) which is hosted at the EBI and the CRG, under accession number EGAS00001003642.

References

Alexander, S.P., Christopoulos, A., Davenport, A.P., Kelly, E., Marrion, N.V., Peters, J.A., Faccenda, E., Harding, S.D., Pawson, A.J., Sharman, J.L., et al; CGTP Collaborators. (2017). THE CONCISE GUIDE TO PHARMACOLOGY 2017/18: G protein-coupled receptors. Br. J. Pharmacol. 174 Suppl 1, S17–S129. https://doi.org/10.1111/bph.13878

Alexandrov, L.B., Nik-Zainal, S., Wedge, D.C., Campbell, P.J., Stratton, M.R. (2013). Deciphering signatures of mutational processes operative in human cancer. Cell Rep 3, 246–259. https://doi.org/10.1016/j.celrep.2012.12.008

Amaral, F.C., Torres, N., Saggioro, F., Neder, L., Machado, H.R., Silva, W.A., Moreira, A.C., Castro, M. (2009). MicroRNAs differentially expressed in ACTH-secreting pituitary tumors. J. Clin. Endocrinol. Metab. 94, 320–323. https://doi.org/10.1210/jc.2008-1451

Anders, S., and Huber, W. (2010). Differential expression analysis for sequence count data. Genome Biology 11, R106. https://doi.org/10.1186/gb-2010-11-10-r106

Anwar, S.L., Wulaningsih, W., Lehmann, U. (2017). Transposable Elements in Human Cancer: Causes and Consequences of Deregulation. Int J Mol Sci 18. https://doi.org/10.3390/ijms18050974

Aryee, M.J., Jaffe, A.E., Corrada-Bravo, H., Ladd-Acosta, C., Feinberg, A.P., Hansen, K.D., Irizarry, R.A. (2014). Minfi: a flexible and comprehensive Bioconductor package for the analysis of Infinium DNA methylation microarrays. Bioinformatics 30, 1363–1369. https://doi.org/10.1093/bioinformatics/btu049

Asa, S.L., Casar-Borota, O., Chanson, P., Delgrange, E., Earls, P., Ezzat, S., Grossman, A., Ikeda, H., Inoshita, N., Karavitaki, N., et al.; attendees of 14th Meeting of the International Pituitary Pathology Club, Annecy, France, November 2016. (2017). From pituitary adenoma to pituitary neuroendocrine tumor (PitNET): an International Pituitary Pathology Club proposal. Endocr. Relat. Cancer 24, C5–C8. https://doi.org/10.1530/ERC-17-0004

Bengtsson, D., Schrøder, H.D., Andersen, M., Maiter, D., Berinder, K., Feldt Rasmussen, U., Rasmussen, Å.K., Johannsson, G., Hoybye, C., van der Lely, A.J., et al. (2015). Long-term outcome and MGMT as a predictive marker in 24 patients with atypical pituitary adenomas and pituitary carcinomas given treatment with temozolomide. J. Clin. Endocrinol. Metab. 100, 1689–1698. https://doi.org/10.1210/jc.2014-4350

Ben-Shlomo, A., Liu, N.-A., Melmed, S. (2017). Somatostatin and dopamine receptor regulation of pituitary somatotroph adenomas. Pituitary 20, 93–99. https://doi.org/10.1007/s11102-016-0778-2

Bergé, L., Bouveyron, C., Girard, S. (2012). HDclassif: An R Package for Model-Based Clustering and Discriminant Analysis of High-Dimensional Data. Journal of Statistical Software 46, 1–29. https://doi.org/10.18637/jss.v046.i06

Bi, W.L., Horowitz, P., Greenwald, N.F., Abedalthagafi, M., Agarwalla, P.K., Gibson, W.J., Mei, Y., Schumacher, S.E., Ben-David, U., Chevalier, A., et al. (2017). Landscape of Genomic Alterations in Pituitary Adenomas. Clinical Cancer Research 23, 1841–1851. https://doi.org/10.1158/1078-0432.CCR-16-0790

Bottoni, A., Zatelli, M.C., Ferracin, M., Tagliati, F., Piccin, D., Vignali, C., Calin, G.A., Negrini, M., Croce, C.M., Degli Uberti, E.C. (2007). Identification of differentially expressed microRNAs by microarray: a possible role for microRNA genes in pituitary adenomas. J. Cell. Physiol. 210, 370–377. https://doi.org/10.1002/jcp.20832

Butz, H., Likó, I., Czirják, S., Igaz, P., Korbonits, M., Rácz, K., Patócs, A. (2011). MicroRNA profile indicates downregulation of the TGFβ pathway in sporadic non-functioning pituitary adenomas. Pituitary 14, 112–124. https://doi.org/10.1007/s11102-010-0268-x

Cancer Genome Atlas Research Network, Weinstein, J.N., Collisson, E.A., Mills, G.B., Shaw, K.R.M., Ozenberger, B.A., Ellrott, K., Shmulevich, I., Sander, C., Stuart, J.M. (2013). The Cancer Genome Atlas Pan-Cancer analysis project. Nat. Genet. 45, 1113–1120. https://doi.org/10.1038/ng.2764

Capper, D., Jones, D.T.W., Sill, M., Hovestadt, V., Schrimpf, D., Sturm, D., Koelsche, C., Sahm, F., Chavez, L., Reuss, D.E., et al. (2018). DNA methylation-based classification of central nervous system tumours. Nature 555, 469–474. https://doi.org/10.1038/nature26000

Cheunsuchon, P., Zhou, Y., Zhang, X., Lee, H., Chen, W., Nakayama, Y., Rice, K.A., Tessa Hedley-Whyte, E., Swearingen, B., Klibanski, A. (2011). Silencing of the imprinted DLK1-MEG3 locus in

human clinically nonfunctioning pituitary adenomas. Am. J. Pathol. 179, 2120–2130. https://doi.org/10.1016/j.ajpath.2011.07.002
Chou, C.-H., Chang, N.-W., Shrestha, S., Hsu, S.-D., Lin, Y.-L., Lee, W.-H., Yang, C.-D., Hong, H.-C., Wei, T.-Y., Tu, S.-J., et al. (2016). miRTarBase 2016: updates to the experimentally validated miRNA-target interactions database. Nucleic Acids Research 44, D239–D247. https://doi.org/10.1093/nar/gkv1258
Cooper, O., Ben-Shlomo, A., Bonert, V., Bannykh, S., Mirocha, J., Melmed, S. (2010). Silent corticogonadotroph adenomas: clinical and cellular characteristics and long-term outcomes. Horm Cancer 1, 80–92. https://doi.org/10.1007/s12672-010-0014-x
D'Angelo, D., Palmieri, D., Mussnich, P., Roche, M., Wierinckx, A., Raverot, G., Fedele, M., Croce, C.M., Trouillas, J., Fusco, A. (2012). Altered microRNA expression profile in human pituitary GH adenomas: down-regulation of miRNA targeting HMGA1, HMGA2, and E2F1. J. Clin. Endocrinol. Metab. 97, E1128-1138. https://doi.org/10.1210/jc.2011-3482
Dobin, A., Davis, C.A., Schlesinger, F., Drenkow, J., Zaleski, C., Jha, S., Batut, P., Chaisson, M., Gingeras, T.R. (2013). STAR: ultrafast universal RNA-seq aligner. Bioinformatics 29, 15–21. https://doi.org/10.1093/bioinformatics/bts635
Dray, S., and Dufour, A.-B. (2007). The ade4 Package: Implementing the Duality Diagram for Ecologists. Journal of Statistical Software 22, 1–20. https://doi.org/10.18637/jss.v022.i04
Drouin, J. (2016). 60 YEARS OF POMC: Transcriptional and epigenetic regulation of POMC gene expression. J. Mol. Endocrinol. 56, T99–T112. https://doi.org/10.1530/JME-15-0289
Duong, C.V., Emes, R.D., Wessely, F., Yacqub-Usman, K., Clayton, R.N., Farrell, W.E. (2012). Quantitative, genome-wide analysis of the DNA methylome in sporadic pituitary adenomas. Endocr. Relat. Cancer 19, 805–816. https://doi.org/10.1530/ERC-12-0251
Escofier, B., and Pagès, J. (1994). Multiple factor analysis (AFMULT package). Computational Statistics & Data Analysis 18, 121–140. https://doi.org/10.1016/0167-9473(94)90135-X
Fortin, J.-P., Labbe, A., Lemire, M., Zanke, B.W., Hudson, T.J., Fertig, E.J., Greenwood, C.M., Hansen, K.D. (2014). Functional normalization of 450k methylation array data improves replication in large cancer studies. Genome Biology 15. https://doi.org/10.1186/s13059-014-0503-2
Freda, P.U., Beckers, A.M., Katznelson, L., Molitch, M.E., Montori, V.M., Post, K.D., Vance, M.L., Endocrine Society. (2011). Pituitary incidentaloma: an endocrine society clinical practice guideline. J. Clin. Endocrinol. Metab. 96, 894–904. https://doi.org/10.1210/jc.2010-1048
Gaujoux, R., and Seoighe, C. (2010). A flexible R package for nonnegative matrix factorization. BMC Bioinformatics 11. https://doi.org/10.1186/1471-2105-11-367
Gu, Y., Zhou, X., Hu, F., Yu, Y., Xie, T., Huang, Y., Zhao, X., Zhang, X. (2016). Differential DNA methylome profiling of nonfunctioning pituitary adenomas suggesting tumour invasion is correlated with cell adhesion. J. Neurooncol. 129, 23–31. https://doi.org/10.1007/s11060-016-2139-4
Hage, M., Viengchareun, S., Brunet, E., Villa, C., Pineau, D., Bouligand, J., Teglas, J.-P., Adam, C., Parker, F., Lombès, M., et al. (2018). Genomic Alterations and Complex Subclonal Architecture in Sporadic GH-Secreting Pituitary Adenomas. J. Clin. Endocrinol. Metab. 103, 1929–1939. https://doi.org/10.1210/jc.2017-02287
Harada, K., Nishizaki, T., Ozaki, S., Kubota, H., Harada, K., Okamura, T., Ito, H., Sasaki, K. (1999). Cytogenetic alterations in pituitary adenomas detected by comparative genomic hybridization. Cancer Genet. Cytogenet. 112, 38–41.
Hayashi, K., Inoshita, N., Kawaguchi, K., Ibrahim Ardisasmita, A., Suzuki, H., Fukuhara, N., Okada, M., Nishioka, H., Takeuchi, Y., Komada, M., et al. (2016). The USP8 mutational status may predict drug susceptibility in corticotroph adenomas of Cushing's disease. Eur. J. Endocrinol. 174, 213–226. https://doi.org/10.1530/EJE-15-0689
Hegi, M.E., Diserens, A.-C., Gorlia, T., Hamou, M.-F., de Tribolet, N., Weller, M., Kros, J.M., Hainfellner, J.A., Mason, W., Mariani, L., et al. (2005). MGMT gene silencing and benefit from temozolomide in glioblastoma. N. Engl. J. Med. 352, 997–1003. https://doi.org/10.1056/NEJMoa043331
Hui, A.B., Pang, J.C., Ko, C.W., Ng, H.K. (1999). Detection of chromosomal imbalances in growth hormone-secreting pituitary tumors by comparative genomic hybridization. Hum. Pathol. 30, 1019–1023.

Jin, Y., Tam, O.H., Paniagua, E., Hammell, M. (2015). TEtranscripts: a package for including transposable elements in differential expression analysis of RNA-seq datasets. Bioinformatics 31, 3593–3599. https://doi.org/10.1093/bioinformatics/btv422

Kober, P., Boresowicz, J., Rusetska, N., Maksymowicz, M., Goryca, K., Kunicki, J., Bonicki, W., Siedlecki, J.A., Bujko, M. (2018). DNA methylation profiling in nonfunctioning pituitary adenomas. Mol. Cell. Endocrinol. 473, 194–204. https://doi.org/10.1016/j.mce.2018.01.020

Lambert, S.A., Jolma, A., Campitelli, L.F., Das, P.K., Yin, Y., Albu, M., Chen, X., Taipale, J., Hughes, T.R., Weirauch, M.T. (2018). The Human Transcription Factors. Cell 175, 598–599. https://doi.org/10.1016/j.cell.2018.09.045

Lan, X., Gao, H., Wang, F., Feng, J., Bai, J., Zhao, P., Cao, L., Gui, S., Gong, L., Zhang, Y. (2016). Whole-exome sequencing identifies variants in invasive pituitary adenomas. Oncol Lett 12, 2319–2328. https://doi.org/10.3892/ol.2016.5029

Lawrence, M.S., Stojanov, P., Polak, P., Kryukov, G.V., Cibulskis, K., Sivachenko, A., Carter, S.L., Stewart, C., Mermel, C.H., Roberts, et al. (2013). Mutational heterogeneity in cancer and the search for new cancer-associated genes. Nature 499, 214–218. https://doi.org/10.1038/nature12213

Lee, S.-T., and Wiemels, J.L. (2016). Genome-wide CpG island methylation and intergenic demethylation propensities vary among different tumor sites. Nucleic Acids Res 44, 1105–1117. https://doi.org/10.1093/nar/gkv1038

Li, H., and Durbin, R. (2009). Fast and accurate short read alignment with Burrows-Wheeler transform. Bioinformatics 25, 1754–1760. https://doi.org/10.1093/bioinformatics/btp324

Ling, C., Pease, M., Shi, L., Punj, V., Shiroishi, M.S., Commins, D., Weisenberger, D.J., Wang, K., Zada, G. (2014). A pilot genome-scale profiling of DNA methylation in sporadic pituitary macroadenomas: association with tumor invasion and histopathological subtype. PLoS ONE 9, e96178. https://doi.org/10.1371/journal.pone.0096178

Lloyd, R.V., Osamura, R.Y., Klöppel, G., Rosai, J., International Agency for Research on Cancer (Eds.). (2017). WHO classification of tumours of endocrine organs, 4th edition. ed, World Health Organization classification of tumours. International Agency for Research on Cancer, Lyon.

Ma, Z.-Y., Song, Z.-J., Chen, J.-H., Wang, Y.-F., Li, S.-Q., Zhou, L.-F., Mao, Y., Li, Y.-M., Hu, R.-G., Zhang, Z.-Y., et al. (2015). Recurrent gain-of-function USP8 mutations in Cushing's disease. Cell Research 25, 306–317. https://doi.org/10.1038/cr.2015.20

Mao, Z.-G., He, D.-S., Zhou, J., Yao, B., Xiao, W.-W., Chen, C.-H., Zhu, Y.-H., Wang, H.-J. (2010). Differential expression of microRNAs in GH-secreting pituitary adenomas. Diagn Pathol 5, 79. https://doi.org/10.1186/1746-1596-5-79

McKenna, A., Hanna, M., Banks, E., Sivachenko, A., Cibulskis, K., Kernytsky, A., Garimella, K., Altshuler, D., Gabriel, S., Daly, M., et al. (2010). The Genome Analysis Toolkit: a MapReduce framework for analyzing next-generation DNA sequencing data. Genome Res. 20, 1297–1303. https://doi.org/10.1101/gr.107524.110

Mete, O., Kefeli, M., Çalışkan, S., Asa, S.L. (2019). GATA3 immunoreactivity expands the transcription factor profile of pituitary neuroendocrine tumors. Mod. Pathol. 32, 484–489. https://doi.org/10.1038/s41379-018-0167-7

Molitch, M.E. (2017). Diagnosis and Treatment of Pituitary Adenomas: A Review. JAMA 317, 516–524. https://doi.org/10.1001/jama.2016.19699

Newey, P.J., Nesbit, M.A., Rimmer, A.J., Head, R.A., Gorvin, C.M., Attar, M., Gregory, L., Wass, J.A.H., Buck, D., Karavitaki, N., et al. (2013). Whole-Exome Sequencing Studies of Nonfunctioning Pituitary Adenomas. The Journal of Clinical Endocrinology & Metabolism 98, E796–E800. https://doi.org/10.1210/jc.2012-4028

Pack, S.D., Qin, L.-X., Pak, E., Wang, Y., Ault, D.O., Mannan, P., Jaikumar, S., Stratakis, C.A., Oldfield, E.H., Zhuang, Z., et al. (2005). Common genetic changes in hereditary and sporadic pituitary adenomas detected by comparative genomic hybridization. Genes Chromosomes Cancer 43, 72–82. https://doi.org/10.1002/gcc.20162

Palumbo, T., Faucz, F.R., Azevedo, M., Xekouki, P., Iliopoulos, D., Stratakis, C.A. (2013). Functional screen analysis reveals miR-26b and miR-128 as central regulators of pituitary somatomammotrophic tumor growth through activation of the PTEN-AKT pathway. Oncogene 32, 1651–1659. https://doi.org/10.1038/onc.2012.190

Popova, T., Manié, E., Stoppa-Lyonnet, D., Rigaill, G., Barillot, E., Stern, M.H. (2009). Genome Alteration Print (GAP): a tool to visualize and mine complex cancer genomic profiles obtained by SNP arrays. Genome Biol. 10, R128. https://doi.org/10.1186/gb-2009-10-11-r128

Rajasundaram, D., and Selbig, J. (2016). More effort - more results: recent advances in integrative "omics" data analysis. Current opinion in plant biology 30, 57–61. https://doi.org/10.1016/j.pbi.2015.12.010

Raverot, G., Burman, P., McCormack, A., Heaney, A., Petersenn, S., Popovic, V., Trouillas, J., Dekkers, O.M., European Society of Endocrinology. (2018). European Society of Endocrinology Clinical Practice Guidelines for the management of aggressive pituitary tumours and carcinomas. Eur. J. Endocrinol. 178, G1–G24. https://doi.org/10.1530/EJE-17-0796

Reincke, M., Sbiera, S., Hayakawa, A., Theodoropoulou, M., Osswald, A., Beuschlein, F., Meitinger, T., Mizuno-Yamasaki, E., Kawaguchi, K., Saeki, Y., et al. (2015). Mutations in the deubiquitinase gene USP8 cause Cushing's disease. Nature Genetics 47, 31–38. https://doi.org/10.1038/ng.3166

Rindi, G., Klimstra, D.S., Abedi-Ardekani, B., Asa, S.L., Bosman, F.T., Brambilla, E., Busam, K.J., de Krijger, R.R., Dietel, M., El-Naggar, A.K., et al. (2018). A common classification framework for neuroendocrine neoplasms: an International Agency for Research on Cancer (IARC) and World Health Organization (WHO) expert consensus proposal. Mod. Pathol. 31, 1770–1786. https://doi.org/10.1038/s41379-018-0110-y

Robinson, J.T., Thorvaldsdóttir, H., Winckler, W., Guttman, M., Lander, E.S., Getz, G., Mesirov, J.P. (2011). Integrative Genomics Viewer. Nat Biotechnol 29, 24–26. https://doi.org/10.1038/nbt.1754

Ronchi, C.L., Peverelli, E., Herterich, S., Weigand, I., Mantovani, G., Schwarzmayr, T., Sbiera, S., Allolio, B., Honegger, J., Appenzeller, S., et al. (2016). Landscape of somatic mutations in sporadic GH-secreting pituitary adenomas. European Journal of Endocrinology 174, 363–372. https://doi.org/10.1530/EJE-15-1064

Rosenthal, R., McGranahan, N., Herrero, J., Taylor, B.S., Swanton, C. (2016). DeconstructSigs: delineating mutational processes in single tumors distinguishes DNA repair deficiencies and patterns of carcinoma evolution. Genome Biol. 17, 31. https://doi.org/10.1186/s13059-016-0893-4

Salomon, M.P., Wang, X., Marzese, D.M., Hsu, S.C., Nelson, N., Zhang, X., Matsuba, C., Takasumi, Y., Ballesteros-Merino, C., Fox, B.A., et al. (2018). The Epigenomic Landscape of Pituitary Adenomas Reveals Specific Alterations and Differentiates Among Acromegaly, Cushing's Disease and Endocrine-Inactive Subtypes. Clin. Cancer Res. https://doi.org/10.1158/1078-0432.CCR-17-2206

Sapkota, S., Horiguchi, K., Tosaka, M., Yamada, S., Yamada, M. (2017). Whole-Exome Sequencing Study of Thyrotropin-Secreting Pituitary Adenomas. J. Clin. Endocrinol. Metab. 102, 566–575. https://doi.org/10.1210/jc.2016-2261

Shin, J.-H., Blay, S., Graham, J., McNeney, B. (2006). **LDheatmap**: An *R* Function for Graphical Display of Pairwise Linkage Disequilibria Between Single Nucleotide Polymorphisms. Journal of Statistical Software 16. https://doi.org/10.18637/jss.v016.c03

Sondka, Z., Bamford, S., Cole, C.G., Ward, S.A., Dunham, I., Forbes, S.A. (2018). The COSMIC Cancer Gene Census: describing genetic dysfunction across all human cancers. Nat. Rev. Cancer 18, 696–705. https://doi.org/10.1038/s41568-018-0060-1

Song, Z.-J., Reitman, Z.J., Ma, Z.-Y., Chen, J.-H., Zhang, Q.-L., Shou, X.-F., Huang, C.-X., Wang, Y.-F., Li, S.-Q., Mao, Y., et al. (2016). The genome-wide mutational landscape of pituitary adenomas. Cell Research 26, 1255–1259. https://doi.org/10.1038/cr.2016.114

Spada, A., Arosio, M., Bochicchio, D., Bazzoni, N., Vallar, L., Bassetti, M., Faglia, G. (1990). Clinical, biochemical, and morphological correlates in patients bearing growth hormone-secreting pituitary tumors with or without constitutively active adenylyl cyclase. J. Clin. Endocrinol. Metab. 71, 1421–1426. https://doi.org/10.1210/jcem-71-6-1421

Stilling, G., Sun, Z., Zhang, S., Jin, L., Righi, A., Kovācs, G., Korbonits, M., Scheithauer, B.W., Kovacs, K., Lloyd, R.V. (2010). MicroRNA expression in ACTH-producing pituitary tumors: up-regulation of microRNA-122 and -493 in pituitary carcinomas. Endocrine 38, 67–75. https://doi.org/10.1007/s12020-010-9346-0

Subramanian, A., Tamayo, P., Mootha, V.K., Mukherjee, S., Ebert, B.L., Gillette, M.A., Paulovich, A., Pomeroy, S.L., Golub, T.R., Lander, E.S., et al. (2005). Gene set enrichment analysis: A

knowledge-based approach for interpreting genome-wide expression profiles. Proceedings of the National Academy of Sciences 102, 15545–15550. https://doi.org/10.1073/pnas.0506580102

Suzuki, M., Egashira, N., Kajiya, H., Minematsu, T., Takekoshi, S., Tahara, S., Sanno, N., Teramoto, A., Osamura, R.Y. (2008). ACTH and alpha-subunit are co-expressed in rare human pituitary corticotroph cell adenomas proposed to originate from ACTH-committed early pituitary progenitor cells. Endocr. Pathol. 19, 17–26. https://doi.org/10.1007/s12022-008-9014-6

Szymas, J., Schluens, K., Liebert, W., Petersen, I. (2002). Genomic instability in pituitary adenomas. Pituitary 5, 211–219.

Välimäki, N., Demir, H., Pitkänen, E., Kaasinen, E., Karppinen, A., Kivipelto, L., Schalin-Jäntti, C., Aaltonen, L.A., Karhu, A. (2015). Whole-Genome Sequencing of Growth Hormone (GH)-Secreting Pituitary Adenomas. The Journal of Clinical Endocrinology & Metabolism 100, 3918–3927. https://doi.org/10.1210/jc.2015-3129

Wang, K., Li, M., Hakonarson, H. (2010). ANNOVAR: functional annotation of genetic variants from high-throughput sequencing data. Nucleic Acids Res. 38, e164. https://doi.org/10.1093/nar/gkq603

Wierinckx, A., Roche, M., Raverot, G., Legras-Lachuer, C., Croze, S., Nazaret, N., Rey, C., Auger, C., Jouanneau, E., Chanson, P., et al. (2011). Integrated genomic profiling identifies loss of chromosome 11p impacting transcriptomic activity in aggressive pituitary PRL tumors. Brain Pathol. 21, 533–543. https://doi.org/10.1111/j.1750-3639.2011.00476.x

Wilkerson, M.D., and Hayes, D.N., (2010). ConsensusClusterPlus: a class discovery tool with confidence assessments and item tracking. Bioinformatics 26, 1572–1573. https://doi.org/10.1093/bioinformatics/btq170

Wu, S., Gu, Y., Huang, Y., Wong, T.-C., Ding, H., Liu, T., Zhang, Y., Zhang, X. (2017). Novel Biomarkers for Non-functioning Invasive Pituitary Adenomas were Identified by Using Analysis of microRNAs Expression Profile. Biochem. Genet. 55, 253–267. https://doi.org/10.1007/s10528-017-9794-9

Yosefzon, Y., David, C., Tsukerman, A., Pnueli, L., Qiao, S., Boehm, U., Melamed, P. (2017). An epigenetic switch repressing Tet1 in gonadotropes activates the reproductive axis. Proc. Natl. Acad. Sci. U.S.A. 114, 10131–10136. https://doi.org/10.1073/pnas.1704393114

A

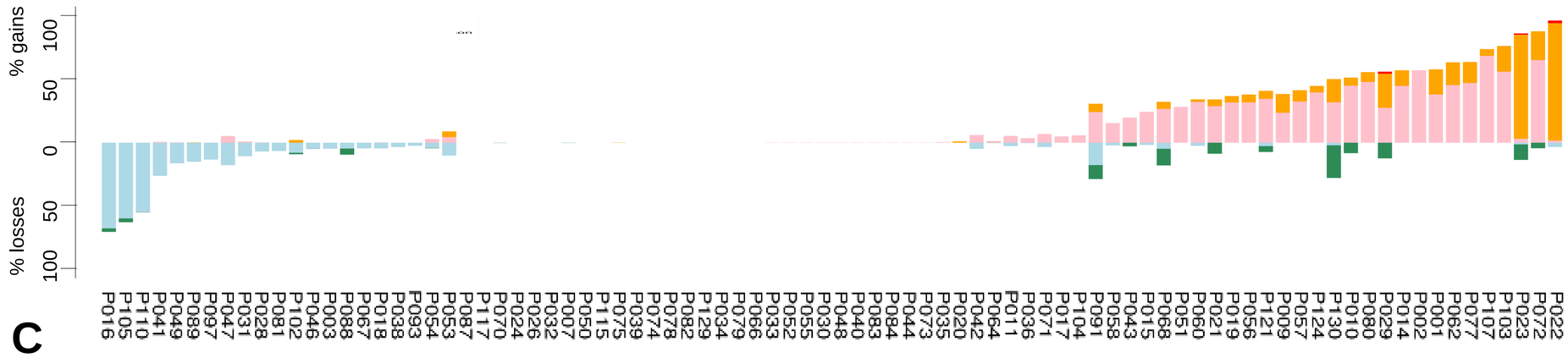

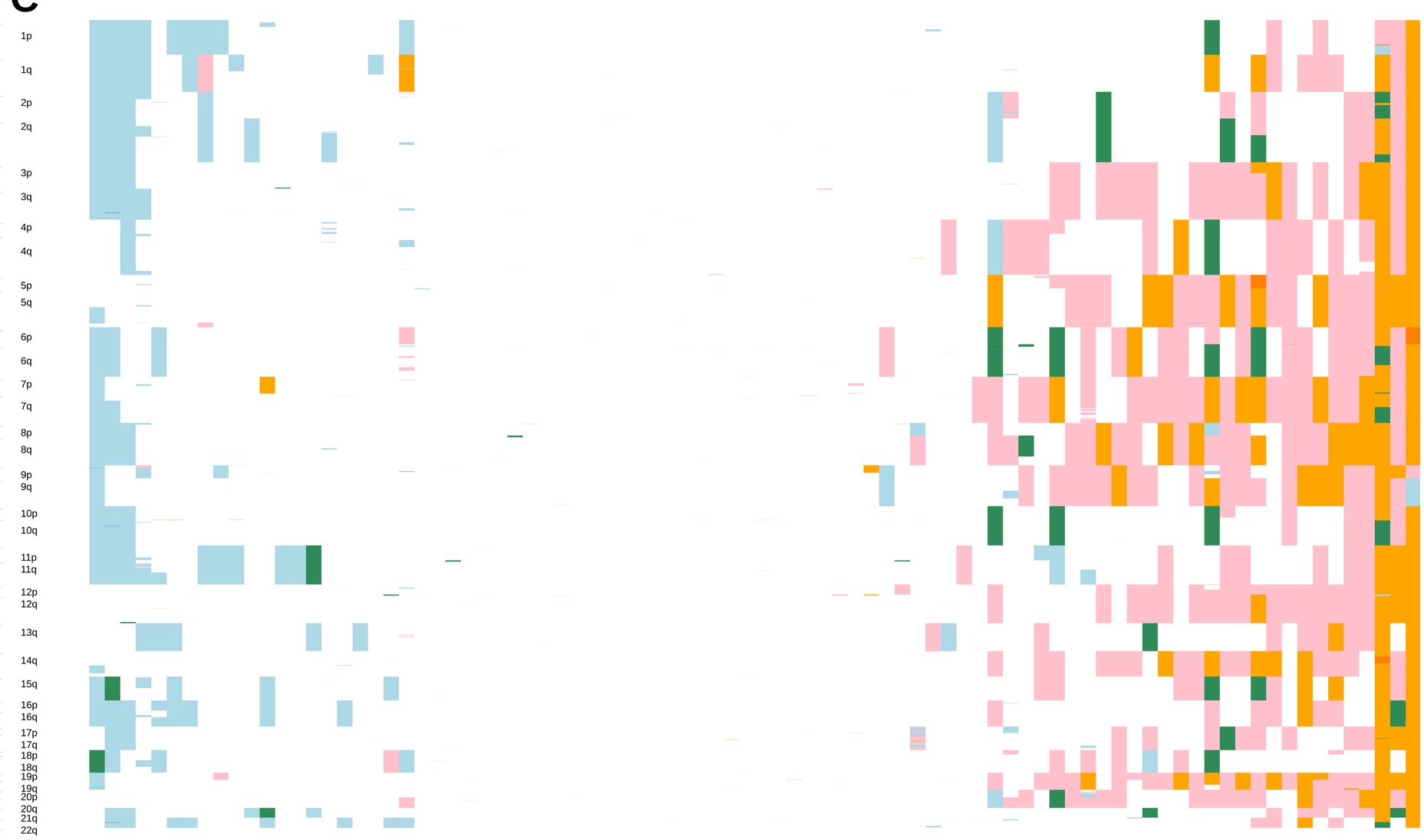

B

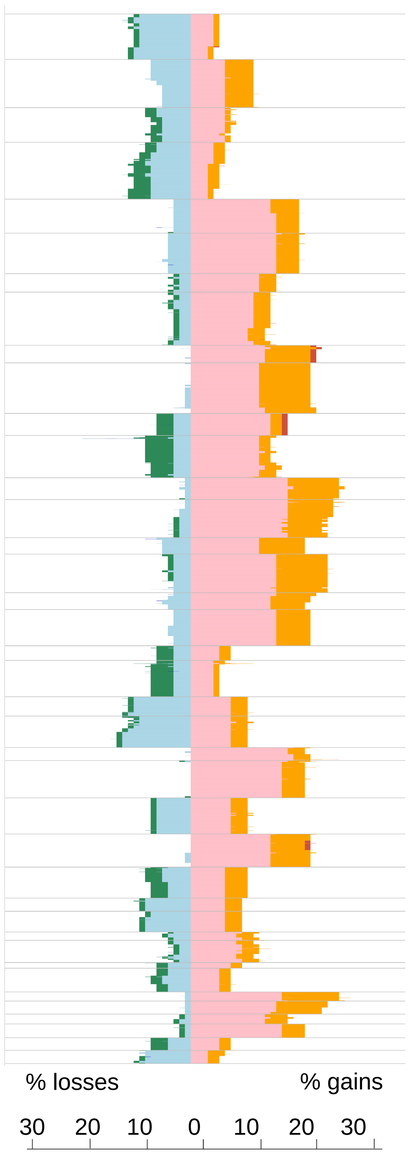

C

D

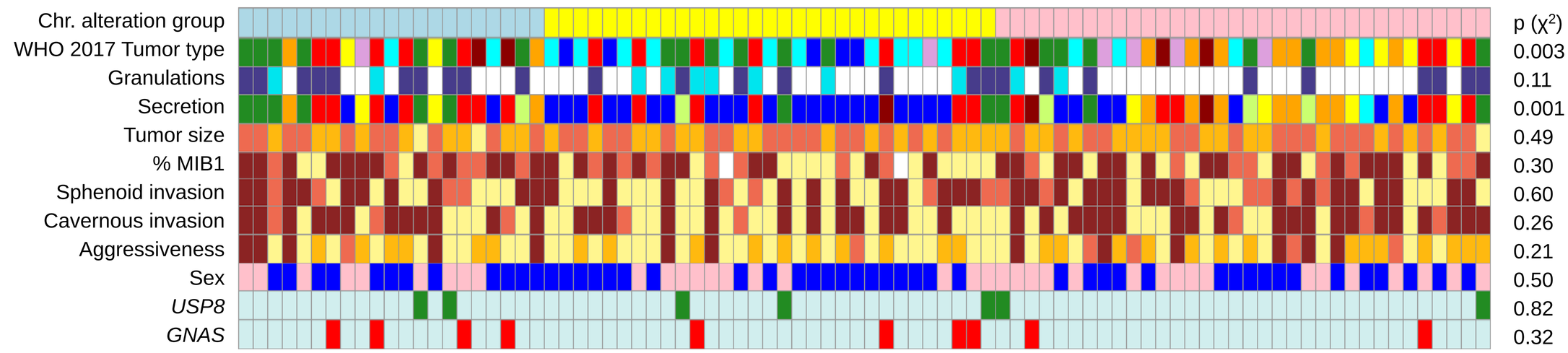

Chr. alteration type
- Loss
- Gain
- Tetraploidy
- Amplicon
- Copy-neutral LOH

Chr. alteration group
- Lost
- Quiet
- Gained

WHO 2017 Tumor type
- Corticotroph
- Lactotroph
- Gonadotroph
- Thyrotroph
- Somatotroph
- Null-cell
- Plurihormonal PIT-1
- Mixed GH-PRL

Secretion
- Overt Cushing
- Subclinical Cushing
- Hyperprolactinemia
- Hyperthyroidism
- Acromegaly
- Mixed
- Silent

Granulations
- Sparse
- Dense
- Not classified

Sex
- Female
- Male

Tumor size
- ≤ 10 mm
- 11-20 mm
- 21-40 mm

% MIB1
- 0-1
- 2
- ≥ 3
- Not available

Sphenoid invasion
- No
- Doubtful
- Yes

Aggressiveness
- Remission
- Persistent
- Resistant
- Aggressive

Cavernous invasion
- No
- Doubtful
- Yes

***USP8* Mutations**
- Yes
- No

***GNAS* Mutations**
- Yes
- No

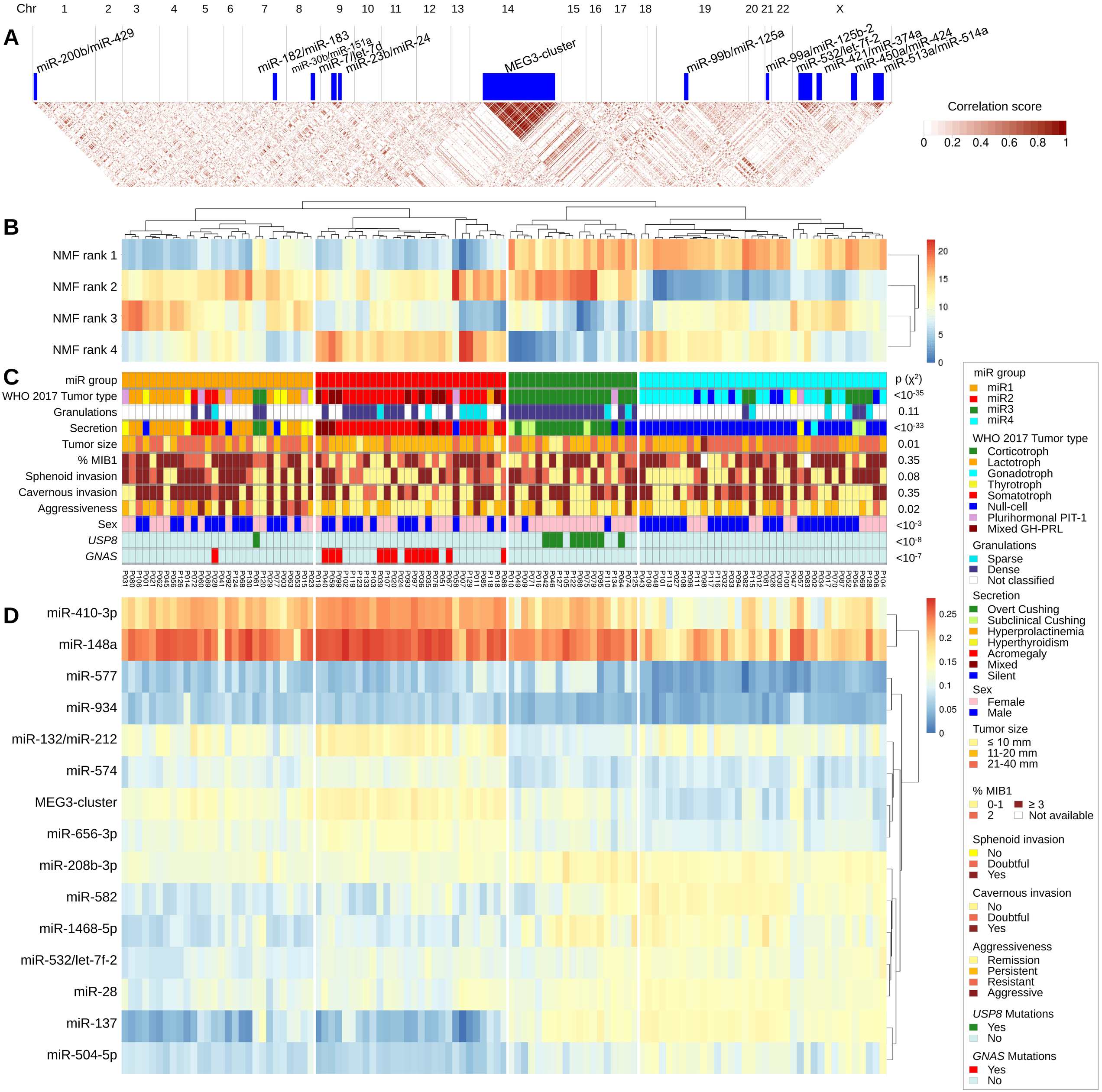
A
Chr 1 2 3 4 5 6 7 8 9 10 11 12 13 14 15 16 17 18 19 20 21 22 X
miR-200b/miR-429
miR-182/miR-183
miR-30b/miR-151a
miR-7/let-7d
miR-23b/miR-24
MEG3-cluster
miR-99b/miR-125a
miR-99a/miR-125b-2
miR-532/let-7f-2
miR-421/miR-374a
miR-450a/miR-424
miR-513a/miR-514a
Correlation score
0 0.2 0.4 0.6 0.8 1
B
NMF rank 1
NMF rank 2
NMF rank 3
NMF rank 4
20 15 10 5 0
C
miR group
WHO 2017 Tumor type
Granulations
Secretion
Tumor size
% MIB1
Sphenoid invasion
Cavernous invasion
Aggressiveness
Sex
USP8
GNAS
p (χ2)
<10-35
0.11
<10-33
0.01
0.35
0.08
0.35
0.02
<10-3
<10-8
<10-7
D
miR-410-3p
miR-148a
miR-577
miR-934
miR-132/miR-212
miR-574
MEG3-cluster
miR-656-3p
miR-208b-3p
miR-582
miR-1468-5p
miR-532/let-7f-2
miR-28
miR-137
miR-504-5p
0.25 0.2 0.15 0.1 0.05 0
miR group
miR1
miR2
miR3
miR4
WHO 2017 Tumor type
Corticotroph
Lactotroph
Gonadotroph
Thyrotroph
Somatotroph
Null-cell
Plurihormonal PIT-1
Mixed GH-PRL
Granulations
Sparse
Dense
Not classified
Secretion
Overt Cushing
Subclinical Cushing
Hyperprolactinemia
Hyperthyroidism
Acromegaly
Mixed
Silent
Sex
Female
Male
Tumor size
≤ 10 mm
11-20 mm
21-40 mm
% MIB1
0-1
≥ 3
2
Not available
Sphenoid invasion
No
Doubtful
Yes
Cavernous invasion
No
Doubtful
Yes
Aggressiveness
Remission
Persistent
Resistant
Aggressive
USP8 Mutations
Yes
No
GNAS Mutations
Yes
No

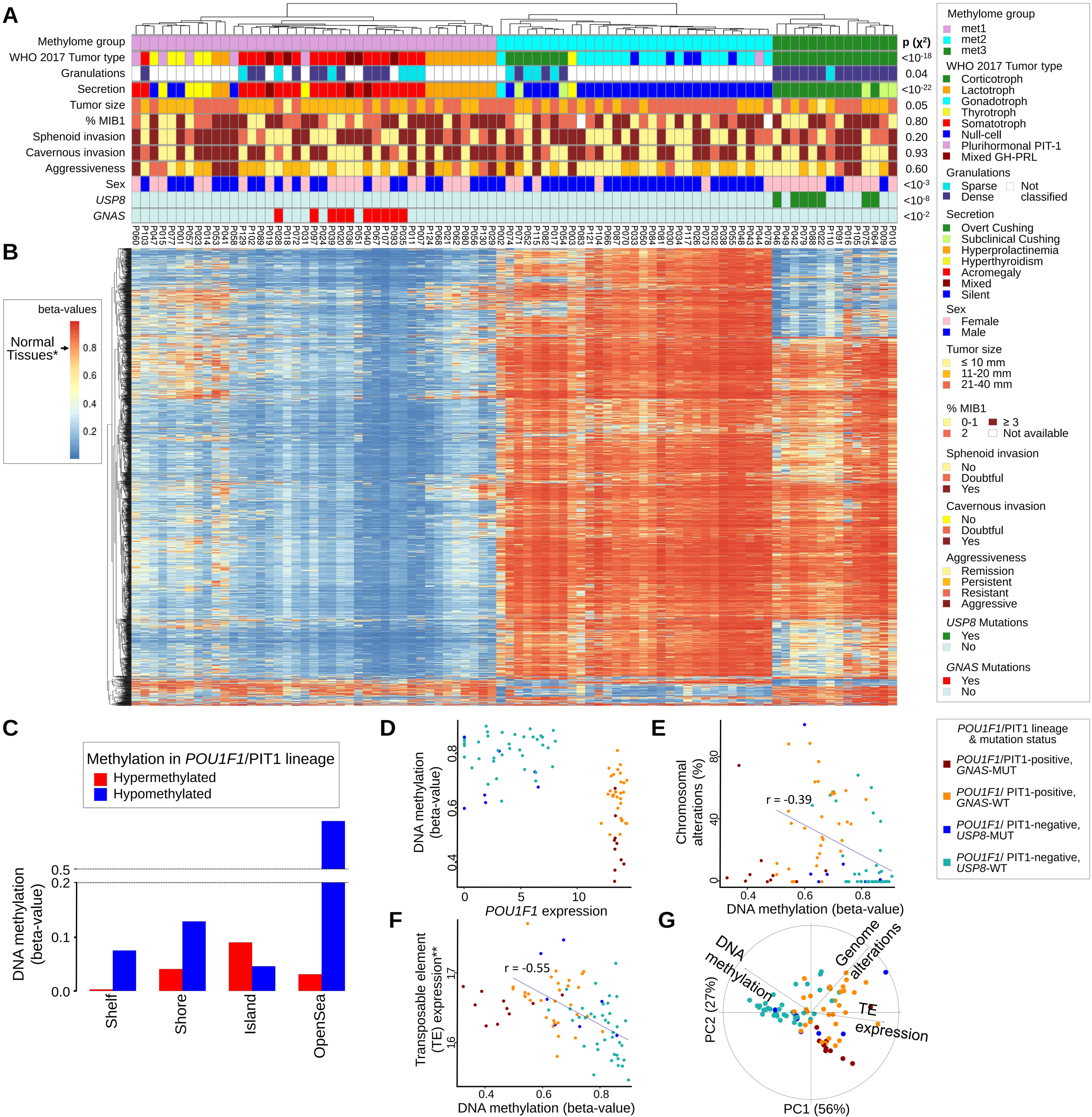
A
Methylome group
WHO 2017 Tumor type
Granulations
Secretion
Tumor size
% MIB1
Sphenoid invasion
Cavernous invasion
Aggressiveness
Sex
USP8
GNAS
p (χ²)
<10-18
0.04
<10-22
0.05
0.80
0.20
0.93
0.60
<10-3
<10-8
<10-2
B
beta-values
Normal Tissues*
0.8
0.6
0.4
0.2
Methylome group
met1
met2
met3
WHO 2017 Tumor type
Corticotroph
Lactotroph
Gonadotroph
Thyrotroph
Somatotroph
Null-cell
Plurihormonal PIT-1
Mixed GH-PRL
Granulations
Sparse
Dense
Not classified
Secretion
Overt Cushing
Subclinical Cushing
Hyperprolactinemia
Hyperthyroidism
Acromegaly
Mixed
Silent
Sex
Female
Male
Tumor size
≤ 10 mm
11-20 mm
21-40 mm
% MIB1
0-1
2
≥ 3
Not available
Sphenoid invasion
No
Doubtful
Yes
Cavernous invasion
No
Doubtful
Yes
Aggressiveness
Remission
Persistent
Resistant
Aggressive
USP8 Mutations
Yes
No
GNAS Mutations
Yes
No
C
Methylation in POU1F1/PIT1 lineage
Hypermethylated
Hypomethylated
DNA methylation (beta-value)
0.5
0.2
0.1
0.0
Shelf
Shore
Island
OpenSea
D
DNA methylation (beta-value)
0.8
0.6
0.4
0
5
10
POU1F1 expression
E
Chromosomal alterations (%)
80
40
0
r = -0.39
0.4
0.6
0.8
DNA methylation (beta-value)
F
Transposable element (TE) expression**
17
16
r = -0.55
0.4
0.6
0.8
DNA methylation (beta-value)
G
DNA methylation
Genome alterations
TE expression
PC2 (27%)
PC1 (56%)
POU1F1/PIT1 lineage & mutation status
POU1F1/PIT1-positive, GNAS-MUT
POU1F1/ PIT1-positive, GNAS-WT
POU1F1/ PIT1-negative, USP8-MUT
POU1F1/ PIT1-negative, USP8-WT

A

p (χ^2)
<10^{-68}
<10^{-4}
<10^{-59}
<10^{-3}
0.17
0.11
0.13
<10^{-3}
<10^{-4}
<10^{-13}
<10^{-9}

mRNA group
WHO 2017 Tumor type
Granulations
Secretion
Tumor size
% MIB1
Sphenoid invasion
Cavernous invasion
Aggressiveness
Sex
USP8
GNAS

B

Rank 4
Rank 1
Rank 3
Rank 2
Rank 6
Rank 5

0.3
0.2
0.1
0

C

Gonadotroph
Corticotroph
Somatotroph
Lactotroph
Thyrotroph

1
0.8
0.6
0.4
0.2
0

E

NKX2-2
ARX
HOXB5
DMRT2
LIN28B
MNX1
SOX11
SOX2
FOXL2
MKX
DMRTA2
ZMAT4
PRDM8
ZNF536
RFX4
SOX5
ESR1
LHX3
KCNIP3
TSHZ2
ISL1
HMGA2
RAX2
ZBED2
ZNF804A
NEUROD1
ASCL1
LMX1A
CUX2
DMRTA1
ZNF750
HIF3A
IRX2
ST18
DACH2
POU1F1
NEUROD4
TBX19
PLAGL1
RORB
AR
PITX2
RXRG
NR5A1
NR0B1
ZFPM2
ZNF385B
FEV
GATA3
GATA2

15
10
5
0

mRNA group
- t1
- t2
- t3
- t4
- t5
- t6

WHO 2017 Tumor type
- Corticotroph
- Lactotroph
- Gonadotroph
- Thyrotroph
- Somatotroph
- Null-cell
- Plurihormonal PIT-1
- Mixed GH-PRL

Granulations
- Sparse
- Dense
- Not classified

Secretion
- Overt Cushing
- Subclinical Cushing
- Hyperprolactinemia
- Hyperthyroidism
- Acromegaly
- Mixed
- Silent

Sex
- Female
- Male

Tumor size
- ≤ 10 mm
- 11-20 mm
- 21-40 mm
- > 40 mm

% MIB1
- 0-1
- ≥ 3
- 2
- Not available

Sphenoid invasion
- No
- Doubtful
- Yes

Cavernous invasion
- No
- Doubtful
- Yes

Aggressiveness
- Remission
- Persistent
- Resistant
- Aggressive

Mutations
- Yes
- No

D

Corticotroph overt Cushing
Corticotroph silent
Gonadotroph

H/E
ACTH
TPIT
SF1
GATA3

P114
P054
P098

A

WHO 2017 Histological Types

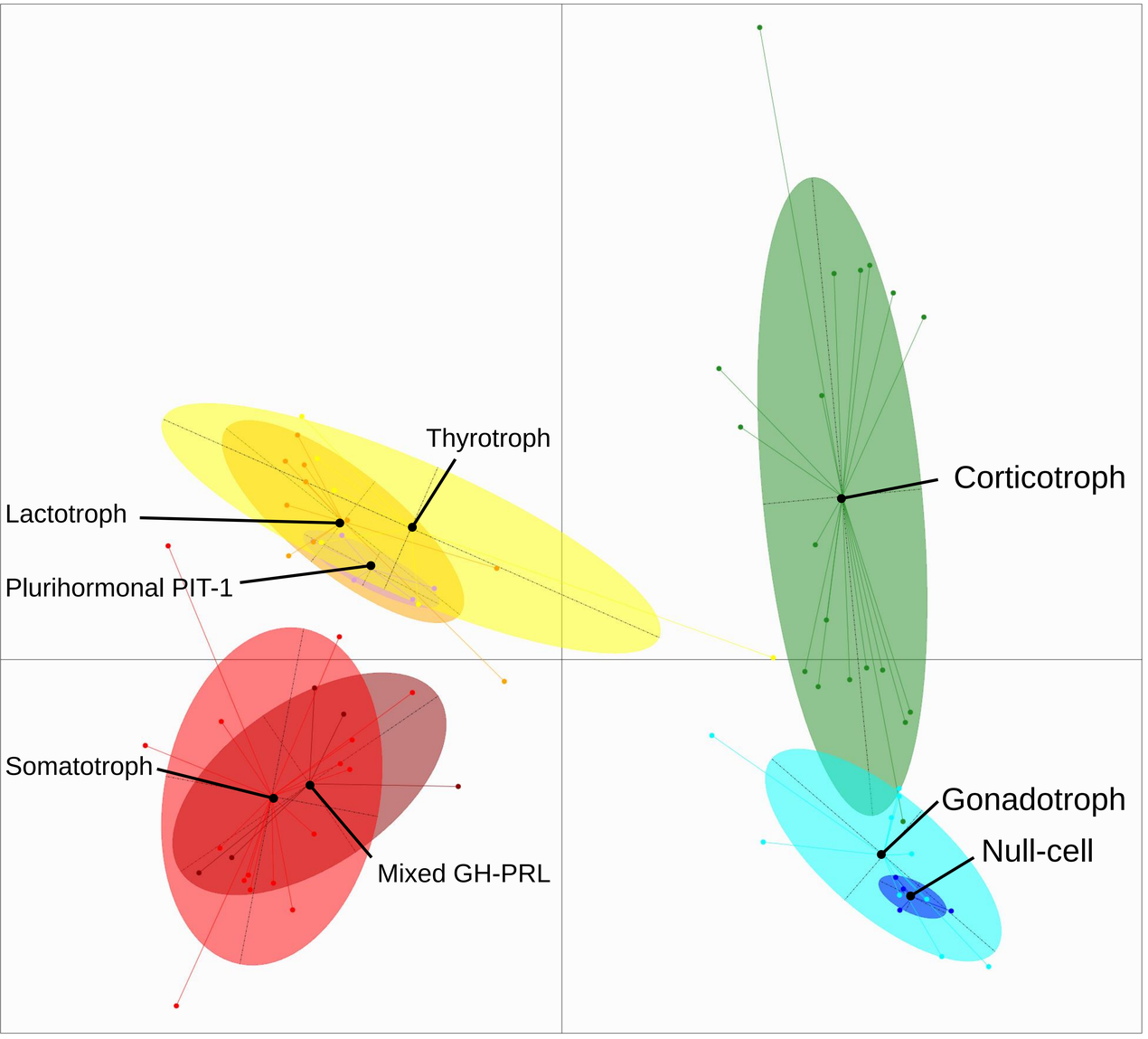

B

Transcriptome Groups

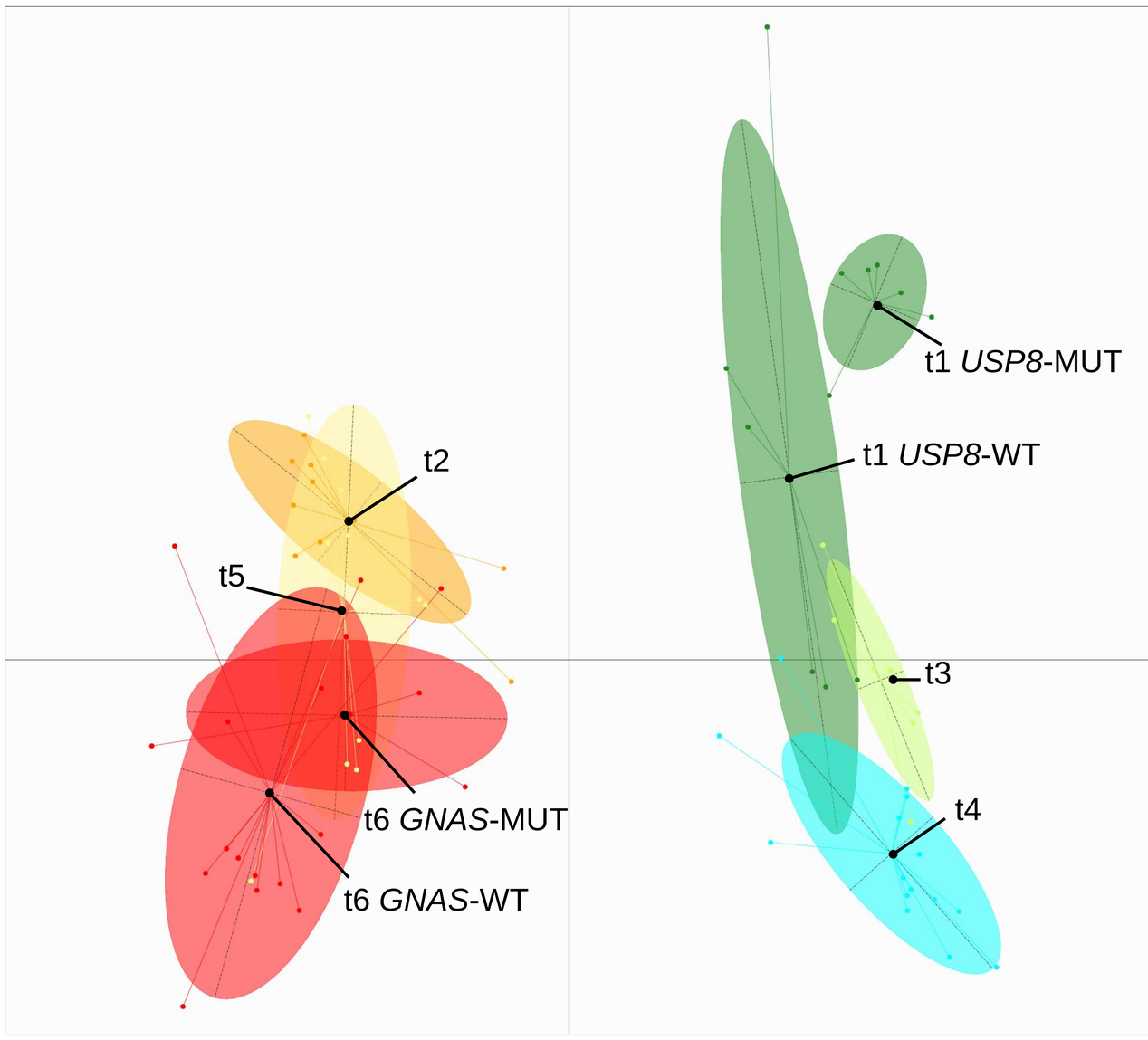

A

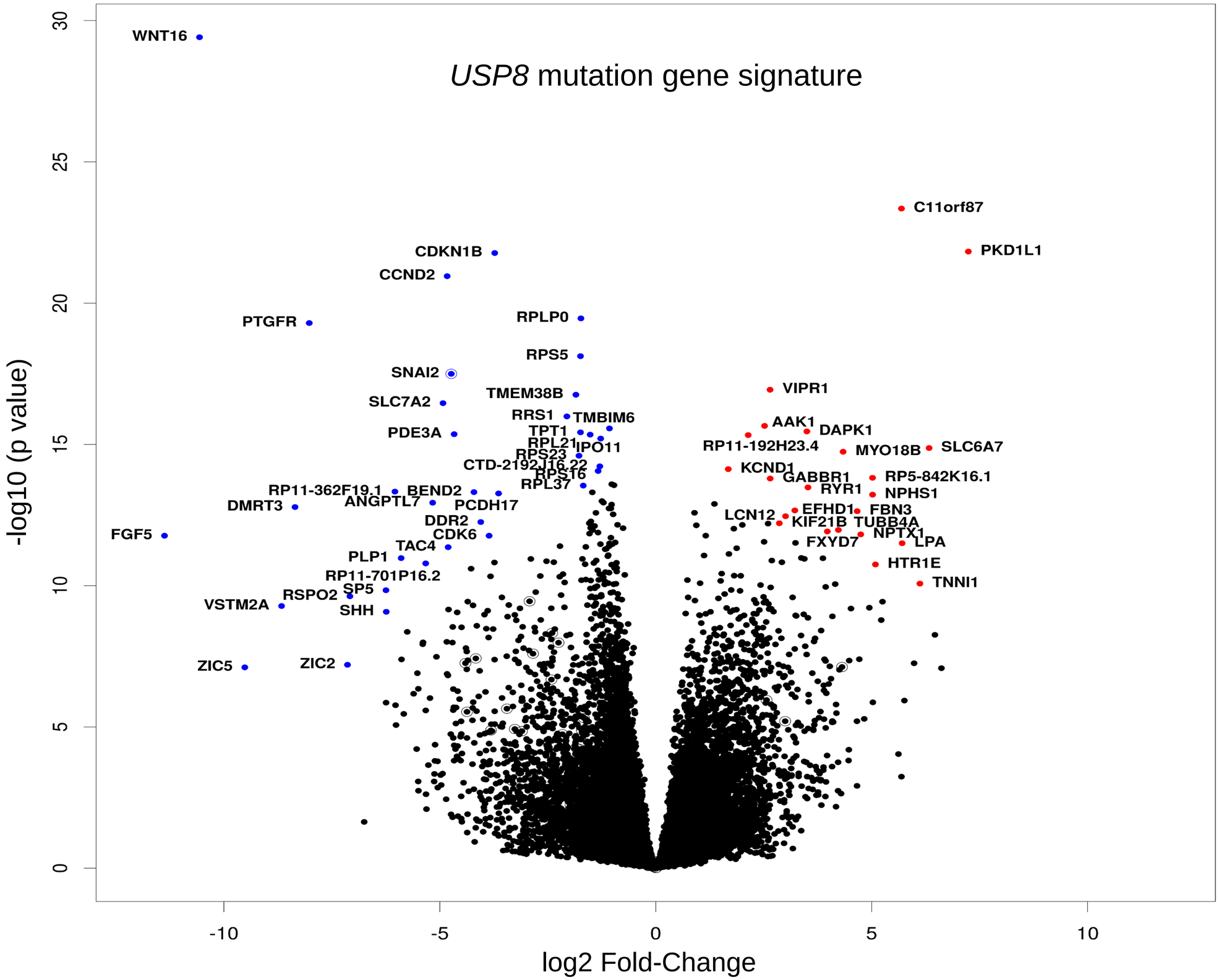
USP8 mutation gene signature
-log10 (p value)
log2 Fold-Change
WNT16
CDKN1B
CCND2
PTGFR
RPLP0
RPS5
SNAI2
TMEM38B
SLC7A2
RRS1
TMBIM6
PDE3A
TPT1
RPL21
IPO11
RPS23
CTD-2192J16.22
RPS16
RPL37
RP11-362F19.1
BEND2
DMRT3
ANGPTL7
PCDH17
DDR2
FGF5
CDK6
TAC4
PLP1
RP11-701P16.2
SP5
RSPO2
VSTM2A
SHH
ZIC5
ZIC2
C11orf87
PKD1L1
VIPR1
AAK1
DAPK1
RP11-192H23.4
MYO18B
SLC6A7
KCND1
GABBR1
RP5-842K16.1
RYR1
NPHS1
LCN12
EFHD1
FBN3
KIF21B
TUBB4A
NPTX1
FXYD7
LPA
HTR1E
TNNI1

B

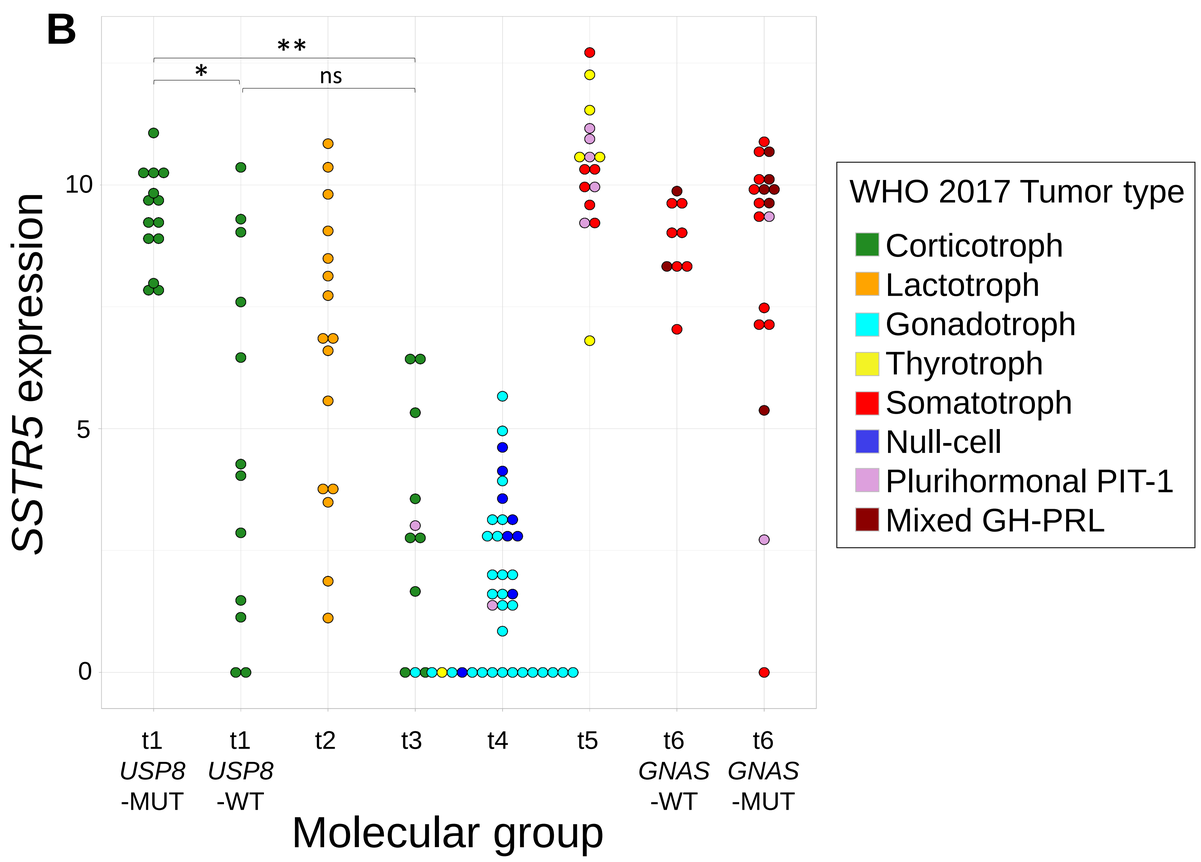
SSTR5 expression
Molecular group
t1 USP8 -MUT
t1 USP8 -WT
t2
t3
t4
t5
t6 GNAS -WT
t6 GNAS -MUT
**
*
ns
WHO 2017 Tumor type
Corticotroph
Lactotroph
Gonadotroph
Thyrotroph
Somatotroph
Null-cell
Plurihormonal PIT-1
Mixed GH-PRL

C

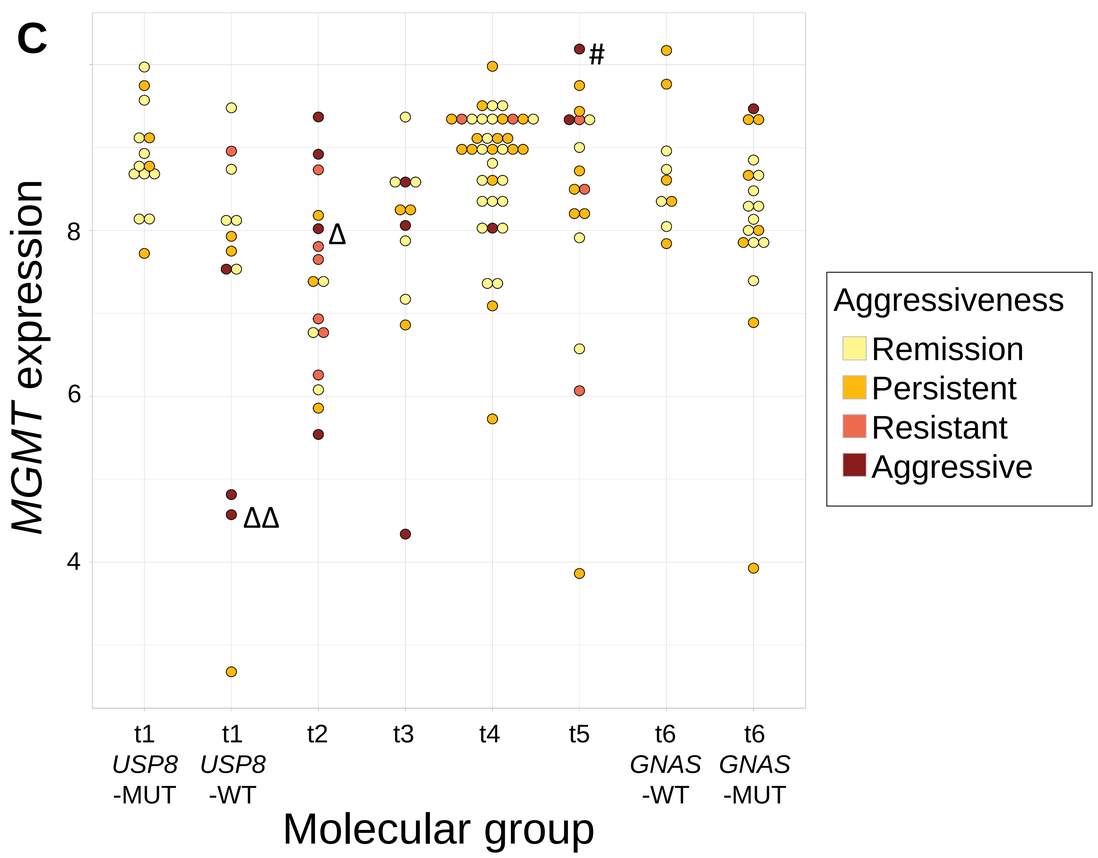
MGMT expression
Molecular group
t1 USP8 -MUT
t1 USP8 -WT
t2
t3
t4
t5
t6 GNAS -WT
t6 GNAS -MUT
#
Δ
ΔΔ
Aggressiveness
Remission
Persistent
Resistant
Aggressive

134 PitNETs

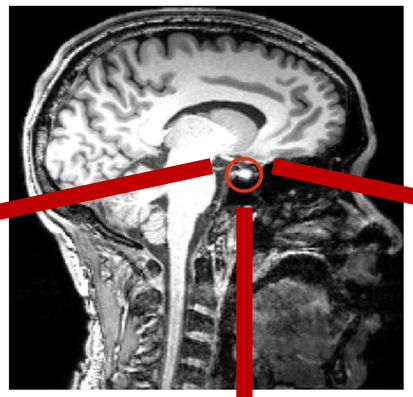

Methylome

Histotype

DNA methylation

POU1F1/PIT1^{+}
Low
DNA methylation

POU1F1/PIT1^{-}
Normal
DNA methylation

Genome

Histotype

Chromosomal alterations

Gained

Quiet

Lost

Cortico *USP8*-MUT

Cortico *USP8*-WT

Lacto

Cortico Silent

Gonado & Null-cell

Thyro

Somato *GNAS*-WT

Somato *GNAS*-MUT

WHO 2017 histotype

Aggressiveness

USP8 mutation

GNAS mutation

% gonadotroph cells

% corticotroph cells

Transcriptome